Delft University of Technology

Aerodynamic Performance Benefits of Over-the-Wing Distributed Propulsion for Hybrid-Electric Transport Aircraft

Vries, Reynard de; Vos, Roelof

Aerodynamic Performance Benefits of Over-the-Wing Distributed Propulsion for Hybrid-Electric Transport Aircraft

Reynard de Vries* and Roelof Vos†

Delft University of Technology, 2629HS Delft, The Netherlands

https://doi.org/10.2514/1.C036909

The goal of this study is to analyze how the aeropropulsive benefits of an over-the-wing distributed-propulsion (OTWDP) system at the component level translate into an aeropropulsive benefit at the aircraft level, as well as to determine whether this enhancement is sufficient to lead to a reduction in overall energy consumption. For this, the preliminary sizing of a partial-turboelectric regional passenger aircraft is performed, and its performance metrics are compared to a conventional twin-turboprop reference for the 2035 timeframe. The changes in lift, drag, and propulsive efficiency due to the OTWDP system are estimated for a simplified unducted geometry using a lower-order numerical method, which is validated with experimental data. For a typical cruise condition and the baseline geometry evaluated in the experiment, the numerical method estimates a 45% increase in the local sectional lift-to-drag ratio of the wing, at the expense of a 12% reduction in propeller efficiency. For an aircraft with 53% of the wingspan covered by the OTWDP system, this aerodynamic coupling is found to increase the average aeropropulsive efficiency of the aircraft by 9% for a 1500 n mile mission. Approximately 4% of this benefit is required to offset the losses in the electrical drivetrain. The reduction in fuel weight compensates for the increase in powertrain weight, leading to a takeoff mass comparable to the reference aircraft. Overall, a 5% reduction in energy consumption is found, albeit with a ± 5% uncertainty due to uncertainty in the aerodynamic modeling alone.

Nomenclature

b	=	span, m
C_D	=	drag coefficient; $D/(q_\infty S_w)$
C_L	=	lift coefficient; $L/(q_\infty S_w)$
c	=	chord, m
c_d	=	sectional drag coefficient; $d/(q_\infty c)$
c_l	=	sectional lift coefficient; $l/(q_\infty c)$
D	=	drag, N; or diameter, m
d	=	sectional drag, N/m
E	=	energy, J
F	=	force, N
h	=	altitude, ft
i_P	=	propeller incidence angle, deg
J	=	advance ratio; $V_\infty/(nD_P)$
L	=	lift, N
l	=	sectional lift, N/m
M	=	Mach number
m	=	mass, kg
N	=	number of propulsors; or normal force, N
n	=	rotational speed, Hz
P	=	power, W
q	=	dynamic pressure; $0.5\rho V^2$, Pa
R	=	range, n mile
S_w	=	wing area, m²
T	=	thrust, N
T_c	=	thrust coefficient; $T/(q_\infty D_P^2/4)$
t	=	time, s
V	=	velocity, m/s
W	=	weight, N
x, y, z	=	Cartesian coordinates, m
α	=	angle of attack, deg
$\Delta(\ )$	=	change with regard to uninstalled conditions
δ_f	=	flap deflection angle, deg
δ_P	=	thrust-vectoring angle, deg
ζ	=	overall efficiency parameter
η	=	component efficiency
η_p	=	propulsive efficiency; $-F_x V_\infty/P_s$
ξ	=	throttle
ρ	=	density, kg/m³
φ	=	shaft-power ratio

Subscripts

airframe	=	airframe-only contribution
bat	=	battery
bL	=	balked landing
cI	=	one-engine-inoperative ceiling
conv	=	conventional configuration
cr	=	cruise
dp	=	distributed-propulsion system
EM	=	electrical machine
f	=	fuel
GT	=	gas turbine
iso	=	isolated
L	=	landing
max	=	maximum
miss	=	nominal mission
opt	=	optimum
SLS	=	sea-level static conditions
s	=	shaft
ssc	=	second-segment climb
P	=	propeller
PL	=	payload
PT	=	powertrain
p	=	pressure-drag component
p	=	propulsive
TO	=	takeoff
1	=	primary powertrain branch
2	=	secondary powertrain branch
∞	=	freestream conditions

*Visiting Researcher, Faculty of Aerospace Engineering, Kluyverweg 1; R.deVries@tudelft.nl. Member AIAA.

†Assistant Professor, Faculty of Aerospace Engineering, Kluyverweg 1; R.Vos@tudelft.nl. Associate Fellow AIAA.

I. Introduction

THE aviation industry is currently responsible for approximately 2.4% of the total anthropogenic carbon dioxide emissions and 3.5% of the effective radiative forcing [1]. Consequently, institutions such as the European Commission [2] and the National Aeronautics and Space Administration (NASA) [3] have set strict sustainability goals to reduce the climate impact of aviation. One way to meet these targets is to improve the efficiency of the propulsion system and its integration with the airframe [4,5]. A key consideration in this sense is the use of alternative energy sources, such as batteries for (hybrid-) electric propulsion [5,6]. However, for large passenger aircraft, fully electric propulsion is not viable without extremely high battery specific energies [7–9], and thus hybrid solutions with only a modest degree of "electrification" are required instead [10]. In these *hybrid-electric propulsion* (HEP) systems, (part of) the power obtained from the energy source(s) is transmitted to the propulsors as electrical power. By taking advantage of the scalability and versatility of electrical systems, the propulsors can be installed at beneficial locations on the airframe in order to increase the aeropropulsive efficiency of the vehicle. This is known as *distributed propulsion* [11].

In this research, a regional passenger aircraft with over-the-wing distributed propulsion (OTWDP) is analyzed for the 2035 timeframe as an alternative to ongoing investigations into leading-edge distributed-propulsion (LEDP) configurations (see, e.g., Refs. [12,13]). A notional example of such an OTWDP system is shown in Fig. 1. Compared to LEDP, the drag reduction associated with over-the-wing propellers [14] can provide substantial improvements in the lift-to-drag ratio [15]. Moreover, over-the-wing propulsion can lead to reduced flyover noise if the wing-shielding capabilities are exploited [16]. Additionally, if the OTWDP system is designed to induce a Coandă effect [17], or is inclined with the flap in low-speed conditions [18], flow separation can be postponed and the high-lift capabilities can be increased. This combination of aerodynamic and acoustic benefits makes OTWDP a suitable candidate to enhance the overall performance of regional HEP aircraft. However, these systems require additional pylons to place the propellers above the wing, and they lead to a nonuniform loading on the propeller disk, which can significantly reduce the propeller efficiency [15,19]. Furthermore, for such configurations, a substantial increase in aeropropulsive efficiency would be required to offset the weight penalty and transmission losses of the associated hybrid-electric drivetrain [20]. Hence, the questions are 1) whether the aerodynamic benefits at the subsystem level lead to a noticeable aerodynamic benefit at the aircraft level, 2) whether the aerodynamic benefit at the aircraft level is sufficient to offset the weight and efficiency losses of the hybrid-electric powertrain, and 3) whether the overall energy-efficiency benefit is sufficient to justify this radical change in the aircraft layout.

The objective of this paper is therefore to analyze how the aeropropulsive benefits of over-the-wing distributed propulsion at the subsystem level translate into an aeropropulsive benefit at the aircraft level, as well as to determine whether this enhancement is sufficient to lead to a reduction in overall energy consumption. For this, a three-step approach is taken. First, an experiment with a simplified geometry is performed to analyze how the aerodynamic interaction between the propeller and wing affects their respective efficiencies. Subsequently, a simplified numerical method is developed to estimate these effects over a wide range of operating conditions and design parameters, which is in turn validated with the experimental data. These exploratory aerodynamic analyses are performed for a simplified geometry without a duct to limit the complexity of the simulations. Finally, the predictions of the numerical method are incorporated in the preliminary-sizing process of a hybrid-electric regional propeller aircraft. This approach is described in Sec. II. A case study is then defined in Sec. III, presenting the top-level aircraft requirements and assumptions, as well as discussing several configuration-related design considerations. The OTWDP configuration is then sized and compared to a conventional twin-turboprop aircraft sized for the same mission in Sec. IV. Finally, Sec. V illustrates how the aeropropulsive efficiency and energy consumption are affected by the main geometrical design parameters and the power-split strategy of the OTWDP system.

II. Methodology

This section describes the approach taken to evaluate the impact of OTWDP at the aircraft level. The method used to size the aircraft is first presented in Sec. II.A. To account for the aerodynamic interaction between the wing and over-the-wing (OTW) propellers, the aerodynamic model described in Sec. II.B is used. Finally, Sec. II.C presents some of the aircraft-level performance metrics used to compare the OTWDP aircraft to a reference configuration.

A. Aircraft Sizing Method

To demonstrate the effect of OTWDP at the aircraft level, a propeller transport aircraft is sized using the preliminary-sizing method described in Ref. [21]. This method is based on the traditional class-I sizing methods [22–24] but has been modified in two ways to account for hybrid-electric and distributed propulsion. First, the point-performance equations are modified to include a series of "delta" terms (ΔC_L, ΔC_D, and $\Delta\eta_p$) representing the aerodynamic interaction between the distributed-propulsion system and the rest of the airframe. Second, a simplified hybrid-electric powertrain model is used to relate the propulsive power requirements to the powers required from each component of the HEP powertrain. These power requirements are represented in a series of component-oriented power-loading diagrams (see Sec. IV). A cross-validation study of the sizing method has been performed in Ref. [25].

In this simplified class-I design approach, the effect of OTWDP is investigated predominantly from an aerodynamic perspective. For this, the ΔC_L, ΔC_D, and $\Delta\eta_p$ terms are estimated based on the main operational and geometrical parameters of the OTWDP system using a surrogate model. The data for the surrogate model are created using the numerical method described in the following section. However, for simplicity, the components of the hybrid-electric powertrain (gas turbines, electrical machines, etc.) are modeled as "black boxes" with a predetermined efficiency and specific power. Moreover, although the weight of these components is accounted for, it is assumed that the structural weight of the airframe is not significantly affected by the HEP and OTWDP systems. On one hand, the OTWDP system would lead to an increase in wing weight because the wing and/or
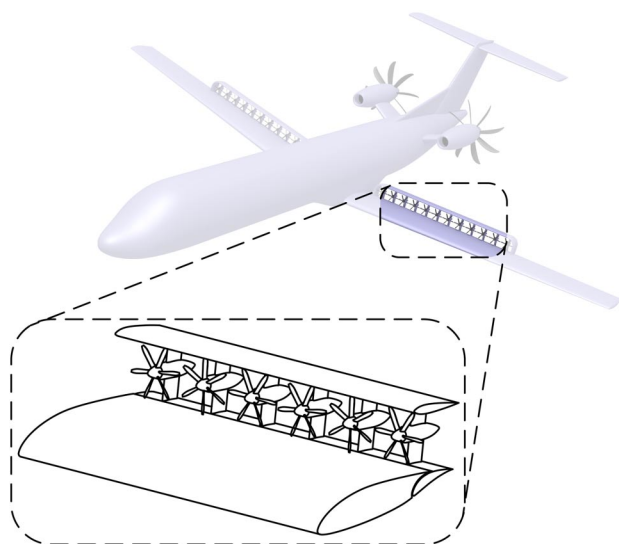
Fig. 1 Example of an over-the-wing distributed-propulsion system (note that figure is for illustrative purposes only; geometry does not represent an optimal design).

flap structure must be able to withstand the forces generated by the propellers, nacelles, pylons, and (potentially) ducts, which may constitute a limiting load case in some designs. The placement of the components of the electric drivetrain may also affect the structural weight of the airframe when compared to a conventional, fully fuel-based configuration. On the other hand, previous studies suggest that distributed-propulsion systems can reduce the wing weight due to an alleviation of the root bending moment [26], as well as the vertical tail size due to reduced one-engine-inoperative (OEI) yawing moments and the possibility to use thrust vectoring for yaw control [27]. Here, in first approximation, it is assumed that these counteracting effects approximately lead to a net zero effect on the structural weight of the airframe. For additional information regarding this sizing approach, the reader is referred to Ref. [21].

B. Aerodynamic Modeling

The changes in lift, drag, and propulsive efficiency due to aerodynamic interaction between the OTW propellers and the airframe are estimated using a low-order numerical tool, which is in turn validated with experimental data. The experimental and numerical approaches are only briefly described in the following subsections to understand how the results of Secs. IV and V are obtained, as well as what the limitations are. For a more complete description, the reader is referred to chapter 8 of Ref. [28]. Given the variety of aerodynamic surfaces involved in an OTWDP system (wing, flap, blades, pylons, nacelles, ducts, etc.; see Fig. 1) and the viscous three-dimensional unsteady nature of the interaction mechanisms, the scope of the aerodynamic model is limited in two main ways. First, the model is limited to cruise conditions (i.e., flap retracted and low/moderate lift and thrust coefficients). Second, only the lifting surfaces responsible for the main aerodynamic loads (that is, the wing

and propellers) are modeled, whereas other elements such as the duct are not included.

1. Experimental Setup

An overview of the experimental setup used in the wind-tunnel tests, performed in the DNW Low-Speed Tunnel (LST), is shown in Fig. 2. In these tests, the effect of three propellers placed above a rectangular wing was quantified using an external balance and pressure taps. The wing model had a chord of $c = 0.3$ m and a span of $b = 1.25$ m, and it featured an NLF-MOD22B airfoil [29,30]. Three XPROP-S propellers ($D_P = 0.2032$) were installed on a support sting on the suction side of the wing. Additional information regarding the propeller geometries can be found in Refs. [31,32]. Furthermore, a ground table was used as the endplate of the wing to reduce tip effects and ensure that the *changes* in wing lift due to propeller interaction at the midspan were representative of the changes that would occur on an infinite wing. Measurements were performed at a relatively low Reynolds number of $6 \cdot 10^5$. However, because the test focused on cruise conditions (flap retracted, attached flow), the resulting data were considered representative for the validation of the numerical method.

2. Numerical Setup

The numerical method combines three main components to model the aerodynamic interaction between wing and propellers, as shown in Fig. 3a:
1) The first component is a propeller-performance model that estimates the changes in loading on the propeller disk due to velocity gradients above the wing. This method divides the disk into radial and azimuthal elements and computes the response of each discretized element to an arbitrary nonuniform inflow using sensitivity maps (e.g., $\partial T_c/\partial J$) obtained from computational fluid

a) Test section seen from upstream

b) Close-up of model
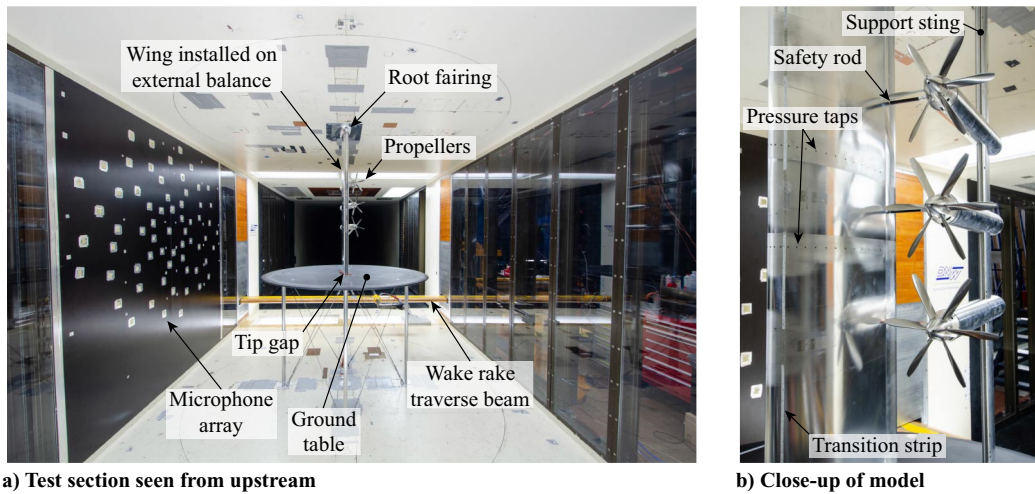
Fig. 2 Overview of the test section and wind-tunnel model used in the experimental campaign.

a) Main components modeled

b) Definition of forces and angles
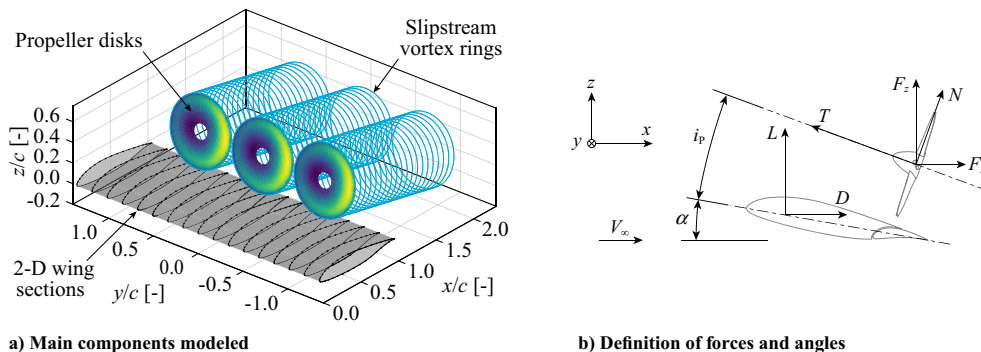
Fig. 3 Overview of the components and forces modeled in the numerical method.

dynamics (CFD) simulations of the propeller geometry in isolated conditions, as described in Ref. [32]. In other words, it allows a rapid calculation of the propeller performance in an arbitrary nonuniform flowfield in installed conditions by using data generated beforehand using a limited number of CFD calculations in uninstalled conditions. Note that, in this study, the propeller-performance estimates are not sensitive to Reynolds and Mach numbers because they are based on sensitivity maps produced for the operating conditions of the experiment. This has a second-order effect on the *changes* in propeller performance due to the interaction, and is considered acceptable for a class-I sizing process. Moreover, the interaction between adjacent propellers is neglected due to the minor effect it has on their performance [31].

2) The second component is a slipstream-vortex model used to estimate the velocities induced by the propeller-vortex system on the wing. By relating the vorticity in the slipstream to the bound circulation on the blades and using the expressions derived by Yoon and Heister [33] to compute the velocity induced by vortex rings, the velocities induced by the propeller-vortex systems at the wing location can be computed analytically.

3) The third component is a series of independent wing sections represented by two-dimensional (2-D) panel methods. Two panel methods are combined: a manual panel-method implementation of linear-strength vortex distributions, following Katz and Plotkin [34], to account for the effect of the propeller-induced velocities; and XFOIL [35] to account for viscous effects. In this quasi-2-D approach, the effect of trailing vorticity due to spanwise variations in wing loading is neglected. This approximation is based on the findings of the experimental campaign, which show that the changes in wing lift and drag beneath the distributed propellers are practically constant in the spanwise direction. Therefore, the changes in induced drag are neglected. Note that OTW propellers are very different from tractor propellers in this regard, where the slipstream impinges on the wing leading edge and the swirl in the slipstream leads to noticeable spanwise loading variations.

Although the effect of the wing on the propeller, and vice versa, is accounted for, no iterative coupling is included. The numerical method is subsequently used to compute Δc_l, Δc_d, and $\Delta \eta_p$ for different thrust coefficients, isolated-wing lift coefficients, Reynolds numbers, Mach numbers, axial propeller positions, diameter-to-chord ratios, and propeller incidence angles. Here, Δc_l and Δc_d refer to the average changes in sectional lift and drag on a wing segment covered by a propeller of the OTWDP system. These sectional coefficients are related to ΔC_L and ΔC_D by multiplying them by the wingspan fraction covered by the OTWDP system, b_{dp}/b. Note that this neglects any changes in wing loading outside the interval covered by the OTWDP system, as well as any changes in induced drag, given that the OTWDP system only has a modest effect on the wing lift distribution. The changes in the overall lift coefficient ΔC_L and drag coefficient ΔC_D are then added to the drag polar of the aircraft, for which a symmetric parabolic polar is assumed. The change in propulsive efficiency $\Delta \eta_p$, on the other hand, is corrected for variable pitch and is added to the propulsive efficiency of the isolated propellers, which is estimated for the same thrust coefficient using actuator-disk theory. To incorporate the delta terms in the sizing process in a computationally efficient manner, a surrogate model is constructed, as described in appendix C of Ref. [28].

3. Applicability and Limitations of the Aerodynamic Model

A validation study has shown that the numerical method captures the physical trends observed in the experiment, and that it provides acceptable estimates of the propeller-induced lift and drag changes in cruise conditions [28]. For $T_c < 0.2$ and $C_L \sim 0.5$, the predicted Δc_l and Δc_{dp} values differ from experimental data by approximately ± 0.02 and ± 0.001, respectively. Moreover, a convergence study of the discretization of the panel methods and slipstream-vortex system showed that, for the selected resolution, the potential deviations in sectional lift and pressure drag from the asymptotic values were on

the order of $\Delta c_l \sim 0.01$ and $\Delta c_{dp} \sim 0.0005$, respectively. No explicit validation of the change in propulsive efficiency was possible with the experimental data; however, additional validation studies performed by van Arnhem et al. [32] suggest that the numerical model is able to capture the changes in propulsive efficiency with an uncertainty on the order of $\Delta \eta_p \pm 0.01$ as compared to full-blade CFD simulations.

Although the validation study showed that the model is useful to predict cruise performance, it also evidenced that the numerical method does not present accurate results if flow separation occurs beneath the propeller. Due to the local propeller-induced adverse pressure gradients, this may occur even if the isolated airfoil presents fully attached flow [17]. For this reason, the aerodynamic model is limited to airframe-only lift coefficients of $C_{L,airframe} < 1$ and thrust coefficients of $T_c < 0.4$. These values are typically exceeded during the mission analysis at the start of climb, as well as for several performance constraints. In that case, the model is likely to provide conservative estimates because the lift and drag benefits increase with thrust setting. Although this implies that the delta terms are inaccurate in these conditions, the conservative approach ensures that the overall potential of OTWDP is not overestimated in this regard. The values obtained at the bounds of the aerodynamic model are also applied to the flight-performance constraints that are performed with the flap deflected (takeoff, approach, and balked landing). This is again considered a conservative approach because earlier research has shown that an OTW propeller can postpone flow separation [17,18] and reduce the pressure drag [30] in the case of flap deflection if the system is properly designed. Although these simplifying assumptions could not be verified within the scope of this research due to the sensitivity of high-lift performance to the Reynolds number and the specific design of the high-lift system, they should be revisited once a more detailed investigation of the high-lift characteristics has been performed.

It is also important to keep in mind that the aerodynamic model does not consider additional elements such as pylons, nacelles, or the duct. Of these elements, especially the duct may play an important role. In this study, the purpose of the OTWDP system is to improve the aeropropulsive efficiency, and hence neglecting the duct can be considered a conservative approach because a duct would only be included if it further enhanced the aeropropulsive efficiency of the system. If, however, noise or fatigue constraints drive the design of the system, then a duct that degrades the aeropropulsive efficiency may be required. Especially in that case, additional research is required to analyze the effect of the duct geometry on system performance. In any case, these considerations indicate that there is some uncertainty regarding the aerodynamic modeling; therefore, in Sec. IV.B, the sensitivity of the aircraft performance metrics to the uncertainty in the aerodynamic model is analyzed.

4. Example: Aerodynamic Performance Benefits at Subsystem Level

Finally, to illustrate how the aerodynamic interaction between the wing and propellers can improve the aeropropulsive efficiency, Fig. 4 presents the lift and drag polars obtained from the external balance in the experimental campaign. Note that the forces refer to the wing only (excluding propellers or support elements) and that roughly 50% of the wingspan is covered by propellers. The figure includes the polars of the clean wing (i.e., with the nacelles and support sting removed) for reference, although a comparison between the propeller-off and propeller-on cases is more representative of the propeller-induced effects because the nacelles and support sting have an arbitrary geometry.

The lift polars of Fig. 4a show how the OTW propellers lead to a slight offset in the lift curve. However, they also lead to a noticeable drag reduction, as evidenced in Fig. 4b. This is a result of the effective angle-of-attack increase and pressure field induced locally beneath the propeller [28]. Consequently, at the lift coefficient corresponding to maximum L/D, the wing lift-to-drag ratio is increased by approximately 23% at a low thrust setting ($J = 1.15$) and by 51% at a high thrust setting ($J = 1.00$). Analogously, for a typical cruise thrust
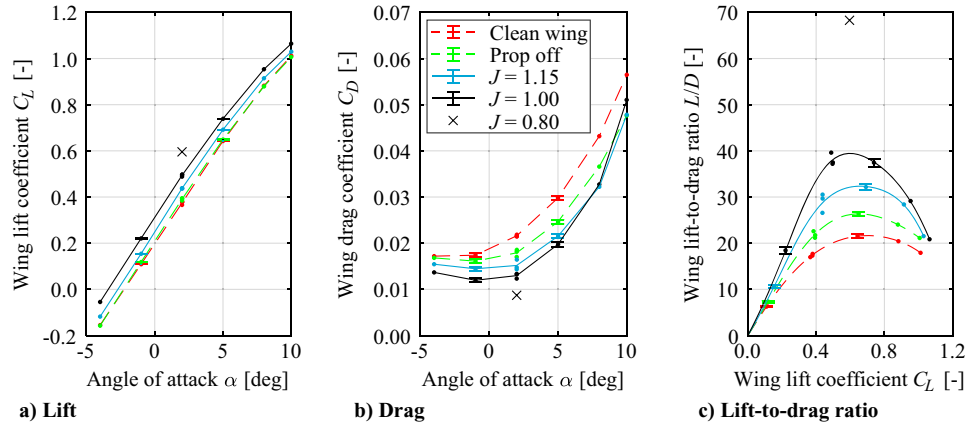
Fig. 4 Wing lift, drag, and lift-to-drag ratio polars. Data obtained from external balance measurements ($x_P/c = 0.8$, $D_P/c = 0.68$). (Prop denotes propeller.)

setting, the numerical method predicts a c_l/c_d increase of approximately 45%, at the expense of a 12% reduction in (propeller) propulsive efficiency. Overall, these results indicate that substantial aeropropulsive benefits can be obtained at the subsystem level. However, these values correspond to a relatively large diameter-to-chord ratio, and they only refer to the lift-to-drag ratio of the wing segment beneath the OTWDP system. Depending on the aircraft configuration, this may or may not lead to a noticeable benefit at the aircraft level. Analogously, the propulsive-efficiency penalty may be less severe at the aircraft level if multiple propulsion systems are considered. These aspects are qualitatively and quantitatively discussed in the following sections.

C. Aircraft Performance Metrics

To understand why the use of OTWDP does or does not lead to a reduction in energy consumption, it is useful to monitor different efficiency metrics of the aircraft. Two important factors in this regard are the lift-to-drag ratio L/D (i.e., the aerodynamic efficiency) and propulsive efficiency η_p, which together form the so-called aeropropulsive efficiency $\eta_p(L/D)$. In the case of the OTWDP system, the propulsive efficiency can be defined as

$$\eta_{p2} = \eta_{p2,iso} + \Delta\eta_p = \frac{-F_x V_\infty}{P_{s2}} \qquad (1)$$

where F_x corresponds to the horizontal force component produced by the propeller (see Fig. 3b), and the subscript "2" indicates that the OTW propellers are part of the secondary, electrically driven powertrain branch. Because the aircraft may present two distinct propulsion systems (see Fig. 1), the average propulsive efficiency can be obtained using the shaft-power ratio φ:

$$\eta_p = \frac{\eta_{p1} + \frac{\varphi}{1-\varphi}\eta_{p2}}{1 + \frac{\varphi}{1-\varphi}} \qquad (2)$$

Moreover, for comparing the overall efficiency of the aircraft, it is of interest to define the powertrain efficiency as the ratio between the total shaft power produced and the total power extracted from the energy sources:

$$\eta_{PT} = \frac{P_{s1} + P_{s2}}{P_f + P_{bat}} \qquad (3)$$

where $P_{bat} = 0$ in the case of a (partial) turboelectric configuration. In this way, an "overall efficiency factor" (also known as the global chain efficiency [36]) of the aircraft can be defined as

$$\zeta = \eta_p \eta_{PT}(L/D) \qquad (4)$$

The parameter ζ is conceptually equivalent to the "range parameter" (see, e.g., chapter 4 of Ref. [37]) but is expressed in terms of

HEP-related parameters instead of the specific fuel consumption of a conventional engine. The parameter appears indirectly in the range equation and is a useful metric for the comparison of distributed-propulsion configurations because, for a given takeoff mass, a reduction in energy consumption with respect to a conventional reference aircraft can only be achieved if $\zeta_{DP} > \zeta_{conv}$. Finally, to quantify the overall energy efficiency of the aircraft, the payload-range energy efficiency (PREE) is used:

$$PREE = \frac{W_{PL}R}{E_{miss}} \qquad (5)$$

where W_{PL} is the payload weight; and R and E_{miss} are the range flown and the energy consumed during the nominal mission (i.e., excluding reserves), respectively. In other words, a higher PREE implies lower energy consumption (and thus lower operating costs and emissions) per passenger kilometer. This parameter is used along with the takeoff mass m_{TO} in Secs. IV and V to compare the overall performance of the OTWDP configuration to the reference aircraft.

III. Case Study Description

In this section, the top-level requirements, design choices, and technology assumptions of the aircraft used to demonstrate the implications of OTWDP are described. First, a set of mission requirements is defined in Sec. III.A. Then, in Sec. III.B, the selected aircraft and powertrain configuration is selected, based on the lessons learned in earlier studies. Finally, the values of the main parameters describing the hybrid-electric/distributed propulsion system are provided in Sec. III.C.

A. Mission Requirements

The results of Ref. [20] highlight that a turboelectric aircraft with distributed propulsion presents a greater advantage over conventional fuel-based aircraft for long-range missions and for low cruise Mach numbers. However, long-haul flights at subsonic cruise speeds are not a realistic scenario due to the significant increase in travel time. Therefore, two missions are considered here. The first is the same mission investigated in Refs. [21,38], which corresponds to the nominal mission of an ATR 72-600 ($M_{cr} = 0.41$, $R = 825$ n miles) [39]. The second corresponds to a high-subsonic turboprop aircraft for longer ranges (see, e.g., the Innovative tubropROp configuratioN (IRON) project; Refs. [40,41]) with a cruise Mach number of $M_{cr} = 0.6$ and a range of $R = 1500$ n miles. A range of 1500 n miles is selected because over 90% of the scheduled passenger flights have ranges below this value [42,43], and such ranges could be covered with lower Mach numbers than those of turbofan aircraft without a significant increase in door-to-door travel time.

A conventional reference aircraft and the OTWDP configuration described in the following section are both sized for these mission requirements. In both cases, the optimum cruise altitude is selected to avoid misleading conclusions regarding the potential of distributed propulsion [38]. The optimum cruise altitudes were found to lie in the intervals of 19,000–22,500 ft and 36,000–40,000 ft for the $M_{cr} = 0.41$ and $M_{cr} = 0.60$ missions, respectively. The optimum cruise altitudes of the $M_{cr} = 0.60$ mission are particularly high as a consequence of the assumed drag polar, which is more representative of low-speed turboprops, and therefore presents the optimum lift-to-drag ratio at an excessively high-lift coefficient for the selected wing loading and cruise Mach number. Although the optimum altitude could be reduced by assuming different drag-polar characteristics for the high-speed case, this was not done in the present study to keep the input variables identical among the two missions. Additionally, for both the short- and medium-range missions, a payload of 7.5 ton (metric tons) (approximately 75 passengers) is considered. Although an increased payload may be beneficial for the longer-range mission, the sensitivity studies of Ref. [20] showed that the change in aircraft performance due to hybrid-electric distributed propulsion is practically insensitive to the payload weight. Therefore, the potential benefits of OTWDP that are analyzed for the chosen payload are also representative for higher payloads.

Several criteria are added to the list of mission requirements considered in Refs. [21,38] to make the design study more representative. First, in addition to the takeoff, cruise, landing, OEI second-segment climb, and OEI ceiling performance constraints, an all-engines operative (AEO) constraint is added following the CS 25.119 regulations [44]. This additional constraint is incorporated because initial investigations showed that the secondary electrical machines, which are not strongly limited by OEI constraints (see Ref. [21]), typically required more power throughout the nominal mission than the value computed in the power-loading diagram. Note that this may even be the case if this additional constraint (or any other) is included, depending on the power-control strategy employed in each flight condition. Moreover, a 30 min loiter at 6,000 ft and a 5% contingency fuel reserve are added. Furthermore, energy fractions are added to account for the fuel employed during startup and takeoff (1.5%) and landing (0.5%) (see part I of the work of Roskam [24]). Finally, the takeoff constraint is computed using the approach described by Torenbeek [45] instead of the takeoff parameter [23] used in previous studies, assuming that all engines are operating during takeoff. In this way, the sensitivity of the takeoff constraint to aerodynamic parameters such as the lift-to-drag ratio are accounted for.

B. Design Considerations for OTWDP Aircraft

The design-space exploration studies of Refs. [20,38] demonstrated that a partial-turboelectric (PTE) powertrain is the most suitable HEP architecture for a regional transport aircraft. This powertrain layout is carried forward in this research, and therefore no batteries are used. It is worth noting that, although this architecture is found to be the best solution in terms of overall energy consumption, in practice, a small amount of batteries could be beneficial or necessary for different reasons: for example, to enable electric taxiing, to reduce emissions in the vicinity of the airport, or to act as a buffer during transient power requirements throughout the mission. However, because the total battery energy capacity has to be minor as compared to the total fuel energy to avoid an excessive weight increase, these effects are not considered for this simplified class-I design study.

A key benefit of the PTE configuration is that a large amount of thrust can be provided by the primary propulsors in the sizing condition, and therefore the electrical components can remain relatively small and light. In the case of a subsonic regional aircraft, the propellers used as primary propulsors have to remain relatively large in order to ensure a low disk loading on both propulsion systems. For example, for an ATR 72-600 [39], the total propeller disk area (24 m^2) equals roughly 40% of the reference wing area (61 m^2). For an OTWDP system to present a comparable disk loading, large diameter-to-chord ratios would be required, which entail significant structural integration challenges. Therefore, in the PTE configuration, a large fraction of the total disk area corresponds to the primary propellers. Thus, the OTWDP system in essence supports the primary propellers with varying levels of power share throughout the mission.

An important consideration for the OTWDP system is which parts of the wing it covers. Although the aerodynamic benefit increases with the span fraction covered, the installation of OTW propulsors in the outboard region comes with several drawbacks, such as an increased roll inertia, increased yawing moments in case of component failure, a potential wing weight increase (depending on the structural sizing condition), and interference with the control surfaces (ailerons). Although the roll control could in principle be provided by means of control surfaces integrated in a duct or stator vane, this additional level of complexity is not considered for the present study. Therefore, the OTWDP system is limited to the inboard portion of the wing, from the root until the outboard edge of the flap. This decision comes with its own challenges because the OTWDP system must be integrated with the flap, and the primary propellers cannot be installed in a typical wing-mounted tractor configuration because their slipstream would cover part of the OTWDP system. Hence, they must be installed on the wingtip, tail, or fuselage. Although each of these positions has its advantages and drawbacks, for the present study, the propellers are placed in a pylon-mounted pusher configuration, similar to the Embraer/FMA CBA-123 Vector [46] or some of the advanced propfan concepts investigated by NASA in the 1980s [47]. This arrangement is

a) OTWDP configuration (top view)

b) OTWDP configuration (front view)
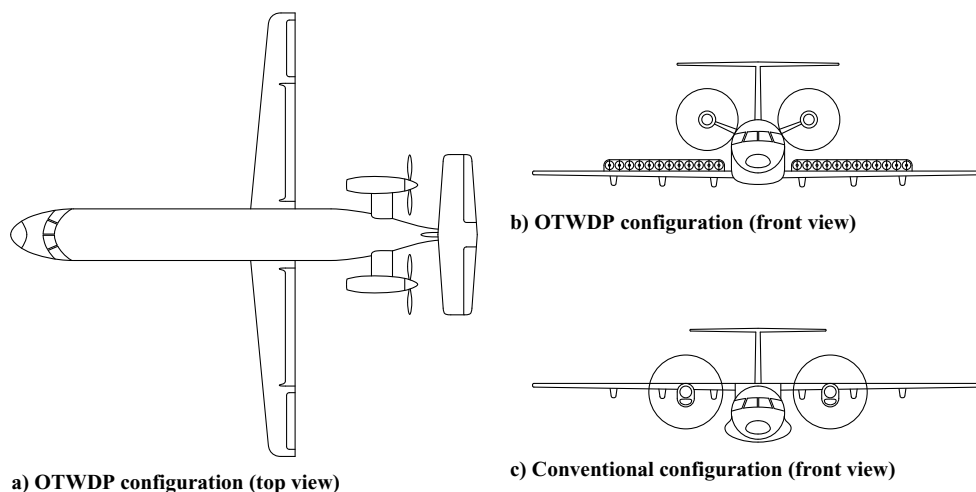
c) Conventional configuration (front view)

Fig. 5   Conceptual sketch of a hybrid-electric regional transport aircraft with OTWDP. Conventional configuration with same total disk area included for reference.

depicted in Fig. 5. At this location, the propellers do not significantly interfere with the horizontal tail, with the ground clearance of the aircraft, or with the wake of the OTWDP system. Moreover, the aft placement of the propellers leads to a reduction in cabin noise as compared to wing-mounted configurations [47]. Although the overall noise levels of the propellers increase due to the impingement of the pylon wake, this penalty could be reduced with a pylon-blowing system [48]. However, this configuration presents a larger center-of-gravity excursion than wing-mounted configurations, which may lead to an increase in tail size, trim drag, and aircraft weight [49]. Although these effects are not accounted for in the class-I sizing phase, they should be kept in mind when assessing the overall performance of the configuration.

Now that the approximate location and extent of the two propulsor systems have been presented, the size and axial position of the OTW propellers have to be decided. Earlier research has shown that the lift-to-drag ratio benefit is higher for propellers placed near the location of maximum airfoil thickness [15,19,30,50]. However, for forward locations, the propulsive efficiency of the propellers is reduced considerably [19,30]. Therefore, for the present study, the OTW propellers are placed near the trailing edge. In this way, the propellers can additionally be installed on the flap. The deflection of the propeller in high-lift conditions can contribute to an effective lift increase due to thrust vectoring (see, e.g., the Lilium concept [51]), as well as postpone flow separation [18]. However, even for $0.75 < x_P/c < 1$, changes in the axial propeller location can appreciably affect the performance of the OTWDP system [30]. The incidence angle of the propeller relative to the wing also plays an important role in this regard: the experimental and numerical analyses described in Sec. II.B show that the performance is improved if the propeller presents a slight nosedown installation angle. Furthermore, although most OTWDP configurations encountered in the literature are ducted [51–53], it is unclear whether a duct is beneficial from an aerodynamic-efficiency perspective. Although the duct can, in principle, reduce the unsteady loading and noise of the propeller (or "fan" in this case), this may not be required for small propellers placed near to the trailing edge. Moreover, although the duct itself contributes positively to thrust at high thrust settings [54,55], in cruise, it is likely to reduce the L/D of the system due to the increase in wetted area [56]. If a duct is required, then a two-dimensional "envelope" duct comparable to the concept of Fig. 5 is considered the best option. A two-dimensional duct is sufficient to reduce the nonuniform inflow because, for an unswept wing, the inflow conditions to the propeller present no significant spanwise variations; and it presents less wetted area and less corner-flow challenges than adjacent circular or square ducts, respectively [28,54]. In any case, further investigation into the effect of the duct shape and position is required.

Based on these criteria, two hypothetical OTWDP arrangements are shown in Fig. 6. In the first (Fig. 6a), the propeller is placed closer to the trailing edge in order to maximize the propeller efficiency. In that case, a duct is not required. However, the propeller must be installed in a pusher configuration.[‡] The impingement of the pylon wake together with the limited wing-shielding capabilities due to the proximity to the trailing edge are likely to lead to an increase in both flyover and cabin noise. In the second configuration (Fig. 6b), the propeller is placed slightly further forward to reduce wing drag. In this case, a duct becomes more advantageous because the wing-induced velocity profile presents stronger gradients. Moreover, if the wavelength of the blade-passage frequency is small relative to the size of the duct or the distance to the wing trailing edge, then this configuration is likely to present lower flyover noise levels than the former due to noise shielding [57]. In both cases, the flap presents a drooped hinge such that a Fowler motion is achieved when rotating the flap. The rotation of the flap is such that, when deflected, the gap is minimized. This leads to a situation comparable to Ref. [18], where the

---

[‡]The terms "pusher" and "tractor" are used in this research to refer to the position of the propeller relative to the motor that drives it, and not relative to the center of gravity of the aircraft.

a) Unducted pusher configuration

b) Ducted tractor configuration

Fig. 6 Conceptual sketch of two OTWDP variants, including the position of the propeller in case of a $\delta_f = 45$ deg flap deflection.

propeller is located behind the suction peak over the flap hinge. It is assumed that, in this configuration, the suction induced upstream by the propeller allows the flow to remain attached without requiring a slot for a fresh boundary layer on the flap. However, further analyses into the interaction effects in high-lift conditions at realistic Reynolds numbers are required to confirm this assumption.

Finally, a generic diameter-to-chord ratio of $D_P/c = 0.25$ is assumed for the sketches of Fig. 6. Existing literature suggests that the wing L/D benefit increases with the diameter-to-chord ratio. However, larger propellers require larger pylons and create a stronger nosedown pitching moment due to the vertical placement of the thrust vector, which can lead to higher actuator loads when installing them on a flap. Although the effect of D_P/c on the aerodynamic performance is accounted for in the following sections, the class-I sizing process is not sensitive to such drawbacks.

C. Propulsion-System Design Parameters and Technology Assumptions

The values of the OTWDP-system design parameters (i.e., geometrical parameters and the power-split strategy) selected for this baseline are provided in Table 1. For both the reference aircraft and the OTWDP configuration, two primary propellers are used ($N_1 = 2$). The size of these propellers is set to $D_{P1}/b = 0.146$ and $D_{P1}/b = 0.126$ for the reference and OTWDP configurations,

Table 1   Design-parameter values assumed for the OTWDP system in the baseline configuration

Parameter	Value
Propeller axial position; x_P/c	0.8
OTWDP wingspan fraction; b_{dp}/b	0.53
Number of secondary propulsors; N_2	24
Propeller incidence angle i_P, deg	0
Thrust-vectoring angle: takeoff $\delta_{P,TO}$, deg	15
Thrust-vectoring angle: landing $\delta_{P,L}$, deg	45
Thrust-vectoring angle: balked landing $\delta_{P,bL}$, deg	45
Shaft-power ratio: cruise φ_{cr}	0.5
Shaft-power ratio: takeoff φ_{TO}	0.2
Shaft-power ratio: landing φ_L	1.0
Shaft-power ratio: OEI second-segment climb φ_{ssc}	0.5
Shaft-power ratio: OEI ceiling φ_{cI}	0.5
Shaft-power ratio: balked landing φ_{bL}	0.5

respectively, such that both configurations have the same ratio between total the propeller disk area and the wing area as an ATR 72-600. For the entire mission analysis, a shaft-power ratio of $\varphi = 0.5$ is assumed. Note that the thrust-vectoring angle in low-speed conditions is treated as a design variable for illustrative purposes. However, in practice, the thrust-vectoring angle would be equal to the angle of attack plus the flap deflection angle, unless a more complicated mechanism is used to provide an additional degree of freedom. Therefore, the propeller–wing–flap system would have to be designed in more detail to ensure that the flap and propeller deflection together lead to a determined overall lift coefficient. The influences of some of these design parameters are discussed in Sec. V. The assumed drag-polar characteristics and other sizing parameters of the aircraft are equal to the values employed in Ref. [38].

For the hybrid-electric powertrain, it is assumed that inverters and rectifiers are required for DC power transmission. Table 2 presents the properties assumed for the powertrain components for the 2035 timeframe. The values are based on current NASA technology development goals [58] and are similar to the values used in Ref. [38]. For this class-I approach, a generic 30% weight penalty is added to the mass of the electrical drivetrain to account for cooling, cables,

Table 2   Assumed powertrain-component properties for the design study

Parameter	Value
Gas-turbine efficiency	0.34
Gearbox efficiency	0.96
Electrical machine efficiency	0.98
Converter efficiency	0.99
PMAD[a] efficiency	0.99
Specific power: electrical machines, kW/kg	13
Specific power: converters, kW/kg	19
PMAD/thermal management weight penalty, %	30

[a]Power management and distribution system.

switches, and other elements of the power distribution and thermal management systems.

IV. Baseline Aircraft Performance

In this section, the aircraft-level performance metrics of a baseline OTWDP configuration are computed. The OTWDP aircraft is first compared to a conventional twin-turboprop reference aircraft in Sec. IV.A. The sensitivity of the aircraft performance to the uncertainty in the aerodynamic model is then assessed in Sec. IV.B.
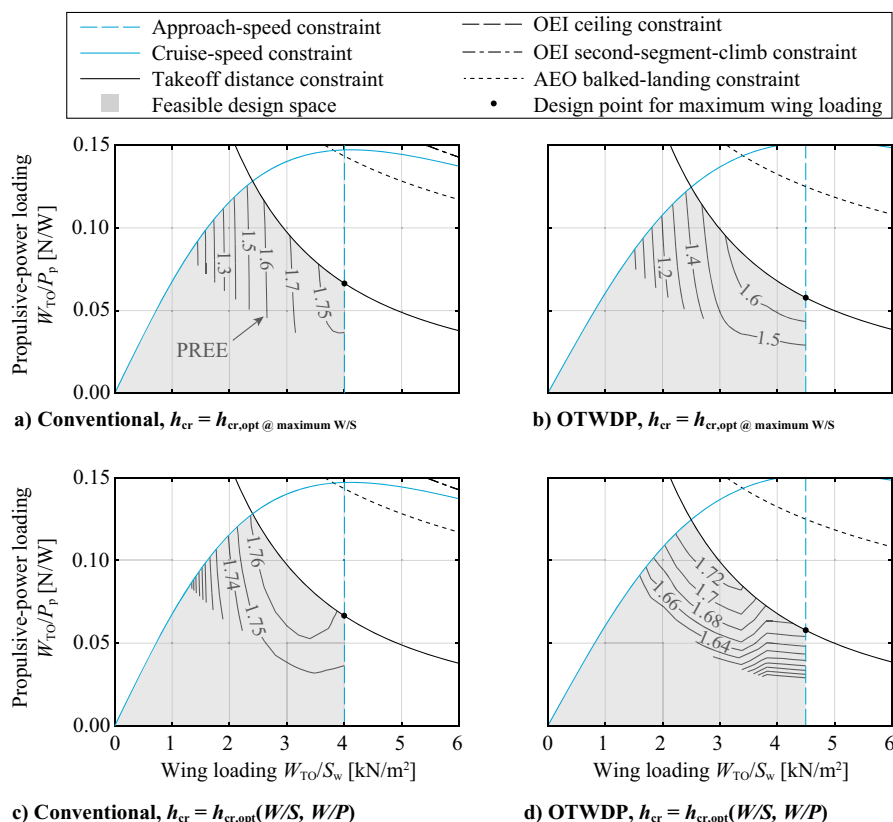
A. Comparison to Reference Aircraft

Figure 7 compares the propulsive-power constraint diagram of the OTWDP aircraft to the one of the conventional reference aircraft. A comparison of Figs. 7a and 7b shows how the approach-speed constraint corresponds to higher wing loadings in the OTWDP configuration due to the effective lift enhancement in landing conditions. Moreover, the cruise constraint allows for slightly higher power loadings in the OTWDP configuration (as observed particularly in the top-right corner of the diagrams) due to the drag reduction of the OTW system. This cruise constraint is performed at the optimum cruise altitude for an aircraft for which the wing loading equals the maximum allowed wing loading: 4.0 and 4.5 kN/m² for the conventional and OTWDP configurations, respectively. The contours of the PREE show that the energy consumption is lowest at the design point of maximum wing loading, as observed in Ref. [38].

However, if the optimum cruise altitude is selected for each feasible combination of wing and power loading, the PREE contours of Figs. 7c and 7d are obtained instead. Note that the cruise constraint at the original cruise altitude of Figs. 7a and 7b is shown in the diagram; although, in reality, the constraint varies, depending on the cruise altitude, and hence on the selected combination of W_{TO}/S_w and W_{TO}/P_p. For lower wing-loading values, the optimum cruise altitude is higher, and thus the actual cruise constraint is less restrictive than the one depicted. In any case, the PREE contours show that the optimum design point changes significantly in this

— — — Approach-speed constraint — — — OEI ceiling constraint
——— Cruise-speed constraint —·—·— OEI second-segment-climb constraint
——— Takeoff distance constraint ········· AEO balked-landing constraint
▢ Feasible design space • Design point for maximum wing loading

a) Conventional, $h_{cr} = h_{cr,opt\ @\ maximum\ W/S}$

b) OTWDP, $h_{cr} = h_{cr,opt\ @\ maximum\ W/S}$

c) Conventional, $h_{cr} = h_{cr,opt}(W/S, W/P)$

d) OTWDP, $h_{cr} = h_{cr,opt}(W/S, W/P)$

Fig. 7   Propulsive power-loading constraint diagrams of conventional reference aircraft (left column) and hybrid-electric OTWDP variant (right column), including contours of PREE obtained in feasible design space for fixed (top row) and optimized (bottom row) cruise altitudes ($M_{cr} = 0.41$).

case. Because the cruise altitude is adapted for each wing loading such that the aircraft operates near the optimum lift-to-drag ratio, the power loading plays a larger role in the location of the optimum design point. This is especially evident for the OTWDP configuration (Fig. 7d), where the optimum design point in terms of the PREE corresponds to a very low wing loading (i.e., a very large wing) and a very high-power loading (i.e., a relatively small powertrain). This effect is more prominent in the OTWDP configuration due to the high powertrain weight fraction for this configuration. In practice, there would be a lower bound on the feasible wing loading because the wingspan is limited by the airport gate category, and the cruise altitude may be restricted by air-traffic constraints. In that case, the characteristics of the drag polar would be adapted to ensure that optimum design point is found at feasible wing-loading values. Given that numerous factors play a role in the location of the optimum design point, the one corresponding maximum wing loading is selected here for further analysis of the baseline configuration. This design choice will be varied in Sec. V.

The corresponding component power-loading diagrams of the gas turbine (GT) and electrical machines of the primary (EM1, i.e., generators) and secondary (EM2, i.e., motors) powertrain branches are shown in Fig. 8. For both the conventional and OTWDP aircraft, the gas turbine is sized by the takeoff requirement for the $M_{cr} = 0.41$ mission, but by the cruise-speed requirement for the $M_{cr} = 0.60$ mission. The gas-turbine power loading of the OTWDP configuration is lower than the conventional configuration because it has to compensate for the power that is dissipated in the electrical drivetrain. This shows that the aerodynamic benefits of the OTWDP system during takeoff do not outweigh the losses in the electrical components. For this reason, a relatively low power share is used during takeoff ($\varphi_{TO} = 0.2$), and the electrical machines are not actively constrained by the takeoff condition. Instead, Fig. 8b shows that

the generators (EM1) are sized by the second-segment-climb constraint in case of component failure because there are only two generators, and thus they have to be oversized by a factor of two. The electrical motors (EM2), on the other hand, are not limited by the OEI constraints because there are numerous motors; in this simplified analysis, it is assumed that only one of them fails in the OEI scenario. Hence, they are sized by the balked-landing constraint.

The aerodynamic, propulsive, and overall efficiencies obtained throughout the nominal mission for the design point of maximum wing loading are shown in Fig. 9. Figure 9a shows that, for the selected OTWDP geometry, the interaction with the wing leads to an appreciable increase in lift-to-drag ratio during climb and cruise. The average propulsive efficiency of the OTWDP aircraft is comparable to the conventional one, being marginally higher during climb due to the higher thrust setting, while being slightly lower during cruise. Note that several factors play a role in the average propulsive efficiency: the efficiency of the primary (tail-mounted) propellers, the isolated-propeller efficiency of the OTWDP system, the change in efficiency of the OTWDP system due to interaction with the wing, and the power split between the two propulsion systems φ. For this comparison, the same total disk area is assumed for the OTWDP and conventional configurations. Therefore, the primary propellers of the OTWDP aircraft are smaller than the ones of the conventional aircraft. If they were the same size, then the overall disk loading of the OTWDP configuration would be lower, leading to a slight increase in propulsive efficiency. Finally, when considering the changes in the lift-to-drag ratio, propulsive efficiency, and powertrain efficiency, the overall efficiency benefit of OTWDP is marginal for the assumed design parameters and component technology levels (Fig. 9c). It is highest during climb, due to the increase in L/D and η_p at higher thrust settings.

The resulting weight breakdown of the two configurations is reflected in Fig. 10. The figure shows that, for both sets of mission

a) Conventional

Powertrain component powers represented in diagrams:
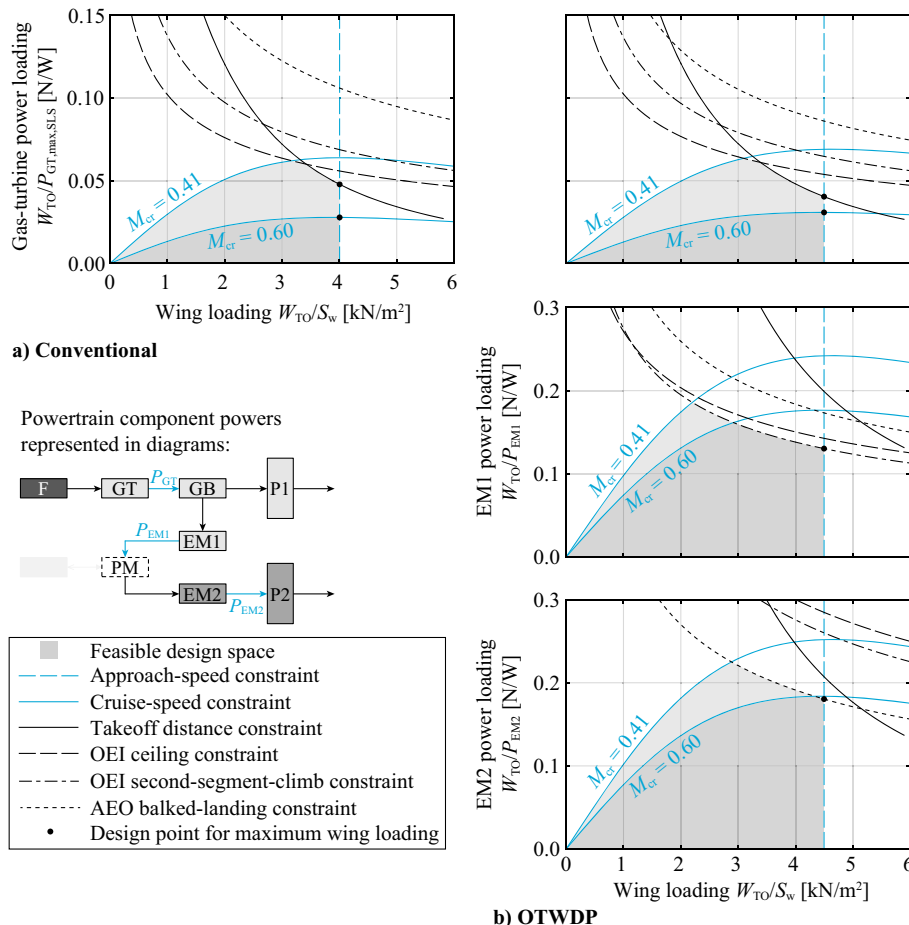
b) OTWDP

Fig. 8 Component power-loading constraint diagrams of the conventional reference aircraft (top left) and the hybrid-electric OTWDP variant (right). (F = fuel, GT = gas turbine, GB = gearbox, PM = power management and distribution system, EM1 = primary electrical machine (generator), EM2 = secondary electrical machine (electric motor), P1 = primary propellers, P2 = secondary propellers).
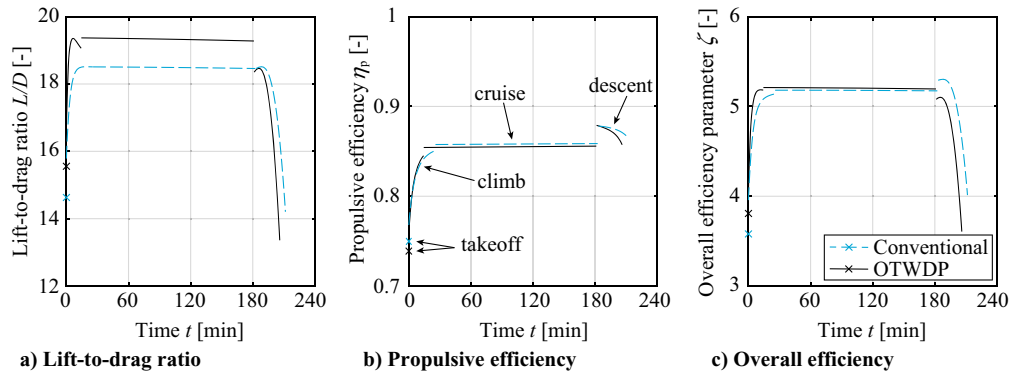
Fig. 9   Aerodynamic, propulsive, and overall efficiencies throughout the nominal mission ($M_{cr} = 0.41$, $R = 825$ n miles). Takeoff values correspond to V_2 (i.e., after liftoff). Diversion and loiter not shown.
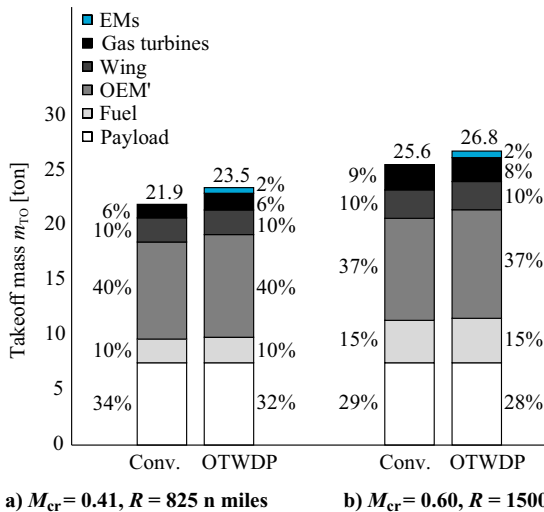
Fig. 10   Mass breakdown of conventional (Conv.) and OTWDP configurations for short- and long-range missions. Values expressed in metric tons and as a percentage of takeoff mass (OEM' = operating empty mass excluding wing and powertrain).

requirements, the minor increase in overall efficiency due to OTWDP is insufficient to offset the increase in takeoff weight; thus, the fuel consumption is slightly higher (in an absolute sense) for the OTWDP configuration. The weight increase is a result of adding the electrical components on one hand, and of requiring a larger gas turbine to offset the losses in the electrical drivetrain (see Fig. 8) on the other. Nevertheless, the differences in takeoff mass and energy consumption between the baseline OTWDP aircraft and the reference aircraft are relatively small.

B.   Sensitivity to Uncertainty in Aerodynamic Modeling

The changes in lift, drag, and propulsive efficiency present some uncertainty for several reasons. First, for a given geometry of the wing and OTW propellers, the numerical model itself presents a determined uncertainty due to the assumptions made in the formulation (modeling error) and the numerical implementation (discretization and convergence errors) of the method. Second, to apply this numerical method, several simplifying assumptions have been made regarding the geometry of the system. Some of these simplifications are likely to contribute to optimistic results (e.g., neglecting nacelles or pylons); some contribute to conservative results (e.g., using a generic, unoptimized wing and propeller geometry); and for others, the effect on overall performance is not fully clear (e.g., the incorporation of a duct). These simplifications are especially important in high-lift conditions, where several additional assumptions have to be made for the method to be applicable in the preliminary-sizing phase (see Sec. II.B.2).

Therefore, to understand how sensitive the aircraft-level performance metrics are to these uncertainties, two hypothetical limit cases are considered: a "conservative" scenario, and an "optimistic" scenario. For the former, the change in lift, drag, and propulsive efficiency are simultaneously decreased, increased, and decreased, respectively. For the optimistic scenario, the opposite is done. For the sectional changes in lift and drag, the deviations from experimental data (indicative of the model error; approximately $\Delta c_l \pm 0.02$ and $\Delta c_d \pm 0.001$) and from the asymptotic value observed in the convergence study (indicative of the discretization error; approximately $\Delta c_l \pm 0.01$ and $\Delta c_d \pm 0.0005$) are added up. These values are scaled by the factor b_{dp}/b (Table 1) to convert them into three-dimensional force coefficients, ΔC_L and ΔC_D. Although the resulting errors (± 0.016 and ± 0.0008 for lift and drag, respectively) may seem small in an absolute sense, they represent errors on the *change* in lift and drag. As shown in Fig. 4, the changes in wing lift and drag due to propeller interaction are approximately $\Delta C_L \sim 0.1$ and $\Delta C_D \sim 0.01$, meaning that these errors are of the order of $\pm 8\%$ to $\pm 16\%$. These levels of accuracy can be expected from a simplified lower-order aerodynamic tool for design-space exploration purposes, but they should not be considered negligible. Finally, for the propulsive efficiency, the indicative error band of $\Delta \eta_p \pm 0.01$ discussed in Sec. II.B.3 is used. An overview of these values is provided for the two scenarios in Table 3.

Figure 11 presents the aircraft performance indicators for the conservative, baseline, and optimistic scenarios. All values are normalized with the corresponding parameter of the conventional reference aircraft. The parameters L/D, η_p, and ζ correspond to average values obtained throughout nominal mission; i.e., diversion and loiter are not included in the metric. Figure 11a shows that the L/D benefit at the aircraft level is doubled and reduced to practically zero for the optimistic and conservative scenarios, respectively. For both sets of mission requirements, the average propulsive efficiency is slightly higher than the reference aircraft in the optimistic scenario, while being lower in the baseline and conservative scenarios. These differences cascade into an overall variation of the PREE of approximately $\pm 5\%$, depending on the mission. The changes in PREE are higher for the long-range mission because the fuel-weight fraction is higher and the aeropropulsive benefit is exploited for a longer duration. Although these variations in PREE ($\pm 5\%$) and takeoff mass ($\pm 3\%$) do not represent a specific confidence interval, they can be considered a conservative

Table 3   Modifications made to the delta terms to analyze the sensitivity to uncertainty in the aeropropulsive model

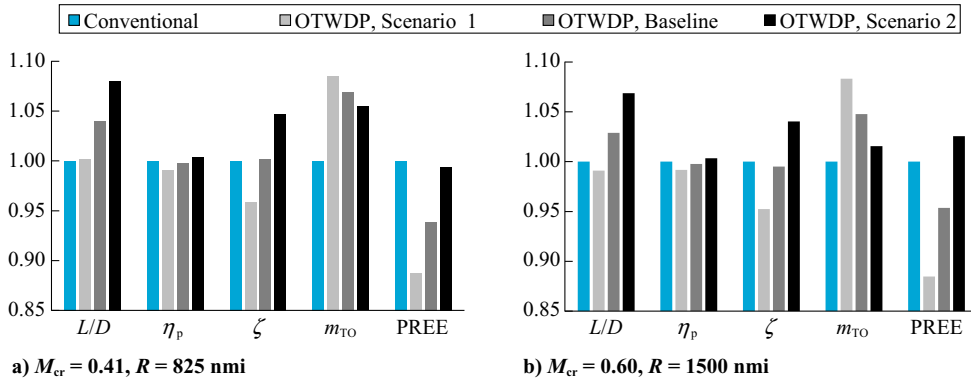|	Scenario 1 (conservative)	Scenario 2 (optimistic)
$\Delta C_L =$	$\Delta C_{L,\text{computed}} - 0.016$	$\Delta C_{L,\text{computed}} + 0.016$
$\Delta C_D =$	$\Delta C_{D,\text{computed}} + 0.0008$	$\Delta C_{D,\text{computed}} - 0.0008$
$\Delta \eta_p =$	$\Delta \eta_{p,\text{computed}} - 0.01$	$\Delta \eta_{p,\text{computed}} + 0.01$

Fig. 11   Effect of aerodynamic-model assumptions on aircraft performance parameters. All values are normalized with the corresponding reference-aircraft values.

indication of the potential error due to uncertainty in the aerodynamic modeling.

V.   Influence of OTWDP Design Parameters

The OTWDP design-parameter values of the baseline configuration analyzed in the previous section were generically selected without any systematic sensitivity or optimization study. Although they provide insight into some of the key effects of OTWDP at the aircraft level, they do not indicate the actual benefit that can be obtained from these systems. The purpose of this section is to investigate how the aircraft-level performance metrics are affected by these parameters. The parameters are divided into two groups: those that define the geometry of the OTWDP system, and those that define the power-split strategy. These two categories are discussed in the two following subsections, respectively. Section V.C then discusses the overall performance of the aircraft with the best combination of OTWDP design-parameter values. Finally, Sec. V.D discusses what the findings imply for potential future applications of OTWDP.

A.   Geometrical Parameters

To investigate the effect of the top-level parameters that describe the geometry of the OTWDP system, the first seven parameters of Table 1 are varied: the axial propeller position; the span fraction covered; the number of propellers; the propeller incidence angle; and the thrust-vectoring angle in the takeoff, landing, and AEO balked-landing constraints. A design-of-experiments (DOE) is performed by distributing 1000 points equally among all dimensions using a Latin-hypercube sampling. The OTWDP aircraft is then sized for the short-range mission ($M_{cr} = 0.41$ and $R = 825$ n miles) for each combination of parameters. The values of these parameters are limited to the bounds specified in Table A2 of the Appendix. The aerodynamic efficiency, propulsive efficiency, takeoff weight, and payload-range energy efficiency of the resulting designs are gathered in Fig. 12. Note that L/D and η_p correspond to the average values obtained throughout the nominal mission.

Figure 12a shows that, even though the design parameters have been limited to "reasonable" bounds, changes in the design of the system can have a significant impact on the aeropropulsive efficiency
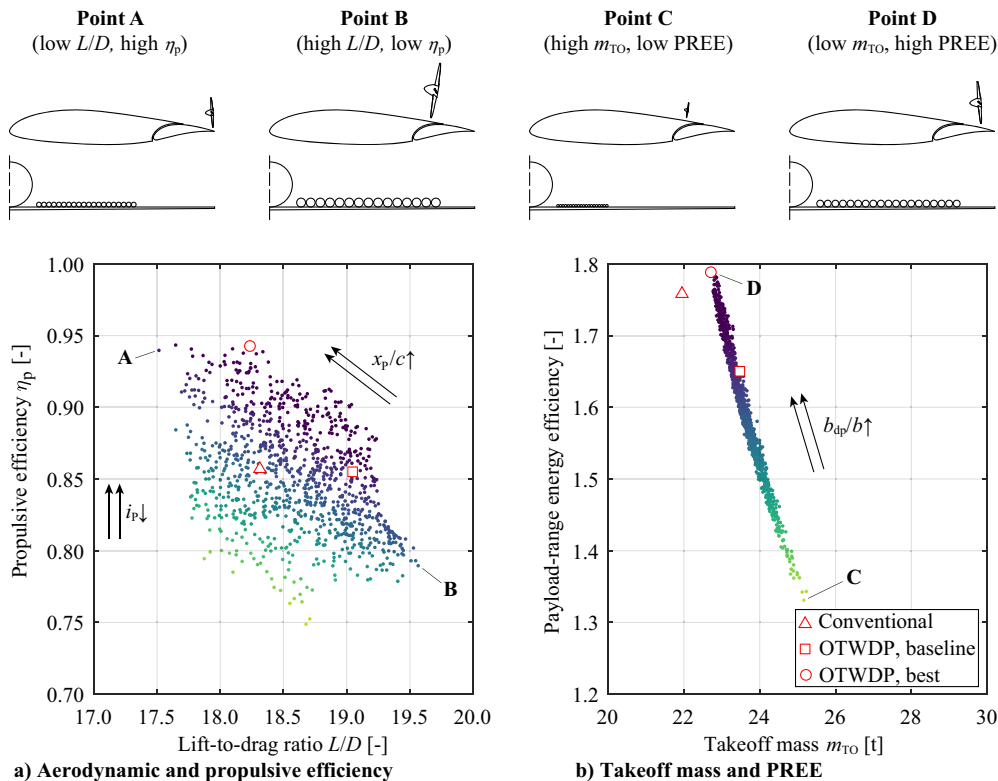

Fig. 12   Top-level aircraft performance metrics for various combinations of OTWDP geometrical design-parameter values as obtained from DOE. Darker colors indicate higher PREE values. Topmost sketches indicate sizes and positions of OTWDP array for four specific data points. $M_{cr} = 0.41$, and $R = 825$ n miles.

of the aircraft. The trends observed at the subsystem level also apply at the aircraft level; for example, a more aft OTW propeller position increases the average η_p of the aircraft but leads to a lower lift-to-drag ratio. Lower propeller incidence angles are also found to increase the average propulsive efficiency. Meanwhile, an increase in the span fraction b_{dp}/b increases the relative influence of the OTWDP system on the overall aerodynamic characteristics of the aircraft, and consequently has a clearly distinguishable effect on the overall energy consumption.

To illustrate these effects, four examples are shown on the top Fig. 12. The point with lowest L/D (point A) also presents roughly the maximum η_p benefit. This design corresponds to a relatively small propeller placed near the trailing edge of the wing, with a small nosedown angle. In this case, a very high average propulsive efficiency can be achieved due to a combination of several factors: the reduction in local velocity near the trailing-edge stagnation point, a small angle-of-attack effect on the propeller that contributes to an increased thrust along the freestream direction, and a decreased disk loading due to a higher total disk area of the aircraft. The opposite occurs for point B, where a series of larger propellers are placed further forward along the chord and along a large fraction of the wingspan. In this case, the lift-to-drag ratio is increased by 7% relative to the conventional aircraft, whereas the propulsive efficiency is reduced by approximately 9%. The design with the lowest PREE (point C), on the other hand, corresponds to an array of small propellers placed upstream of the flap, covering a relatively small portion of the wing. Finally, the design that leads to the lowest energy consumption (point D) corresponds to an array that covers a large portion of the wing, with propellers that present a negative incidence angle and for which the axial position is a compromise between the propulsive-efficiency gain obtained near the trailing edge and the drag reduction obtained at more forward positions.

B. Power-Control Strategy

The power-control parameters of a PTE architecture are the gas-turbine throttle and the shaft-power ratio. The former determines roughly how much thrust the propulsion system produces, whereas the latter determines the thrust share between the primary propellers and the OTWDP system. Therefore, for a given thrust setting, the shaft-power ratio affects the aeropropulsive efficiency of the aircraft. To investigate the effect of the shaft-power ratio φ, a DOE with 1000 data points is performed similarly to the previous section. In this DOE, the φ values of the six performance constraints and of the climb, cruise, descent, and loiter phases of the mission analysis are varied between zero and one. A linear evolution of φ is assumed for

each mission segment, and the same values are applied for the nominal mission and the diversion. The full list of variables is provided in the Appendix (Table A2). In this analysis, the geometrical design parameters of the baseline configuration are maintained (i.e., the best results of the previous section are not used as starting point).

Figure 13 shows the aircraft performance metrics obtained for each combination of shaft-power ratios. For this OTWDP-system geometry, the propulsive efficiency of the aircraft does not vary significantly with φ when compared to the effect of the geometrical design parameters (Fig. 12a). However, the lift-to-drag ratio does vary, and it is particularly sensitive to the shaft-power ratio during cruise. This occurs because higher φ_{cr} values lead to higher OTWDP-system thrust coefficients during cruise, and therefore to an increase in L/D during a large part of the mission. Nevertheless, the colors of the data points show that a higher L/D does not necessarily correspond to a more efficient aircraft in terms of the PREE. The reason for this is that the shaft-power ratio not only affects the aeropropulsive efficiency throughout the mission but also the power requirements of the powertrain components in the constraint diagrams. Therefore, the takeoff mass of the aircraft is much more sensitive to changes in the power-control strategy (Fig. 13b) than to changes in the geometrical parameters of the OTWDP system (Fig. 12b). The shaft-power ratio during takeoff is found to have a particularly large influence on the takeoff mass and, consequently, on the PREE because, in many cases, the takeoff is the limiting constraint for the powertrain components.

In Fig. 13a, the lift-to-drag ratio is more sensitive to the power-control strategy than the average propulsive efficiency. However, a different trend may be observed for a different geometry if, for example, small propellers are placed close to the trailing edge. To ensure that the overall performance comparison between the OTWDP configuration and the reference aircraft is representative, a third and final DOE is performed, where both the geometrical and power-control parameters are varied simultaneously. In this case, the wing loading is also treated as a design variable because the results of Fig. 7 show that the OTWDP configuration may present a strongly suboptimal performance at maximum wing loading. Additionally, the span fraction of the OTWDP system is kept constant and equal to the baseline value because, in this class-I approach, the optimum would be $b_{dp}/b = 1$; but, this is unfeasible due to the space required for the fuselage and ailerons. This leads to a total of 21 design variables, which can be found in Table A2 of the Appendix. The resulting design with maximum PREE is selected for further analysis. For simplicity, that design is referred to as the "optimum" in subsequent paragraphs; however, it should be noted that this corresponds to a well-performing design (as was confirmed

a) Aerodynamic and propulsive efficiency
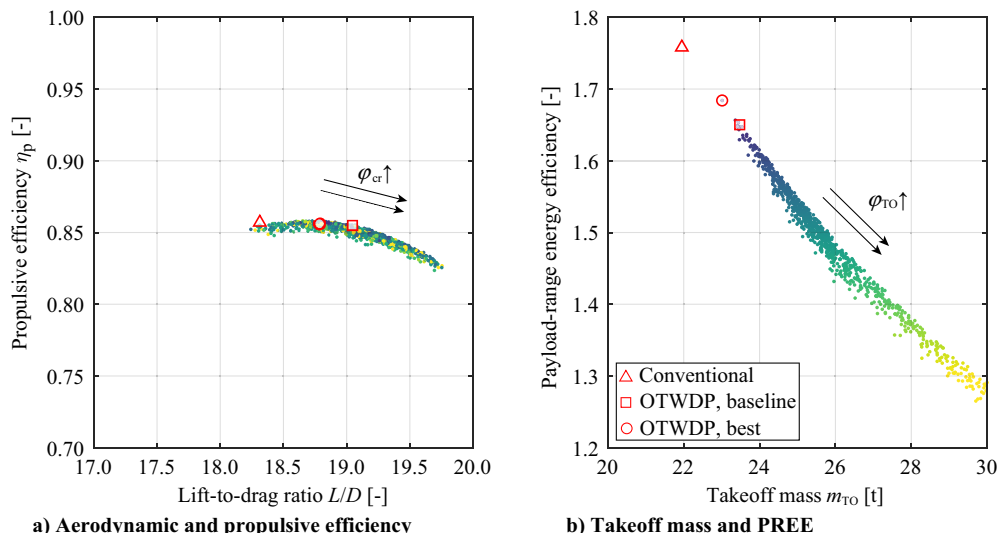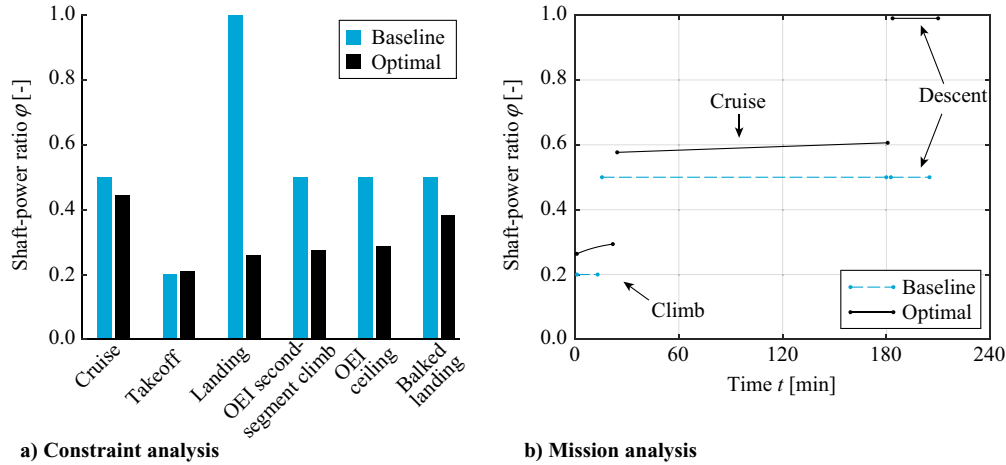
b) Takeoff mass and PREE

Fig. 13 Top-level aircraft performance metrics for various combinations of shaft-power ratio φ as obtained from the DOE. Darker colors indicate higher PREE values. $M_{cr} = 0.41$, and $R = 825$ n miles.

a) Constraint analysis   b) Mission analysis

Fig. 14 Comparison of shaft-power-ratio values obtained for the OTWDP configuration in the performance constraints (left) and throughout the nominal mission (right). $M_{cr} = 0.41$ and $R = 825$ n miles.

in posterior manual evaluations), and not to a global optimum. Also note that the conventional reference aircraft is kept constant because all design variables are only applicable to the OTWDP system. One exception is the design wing loading, but a different wing loading would lead to only minor improvements in the PREE for the conventional aircraft, as reflected in Fig. 7c.

The best-performing power-control strategy obtained from the DOE is shown in Fig. 14. The shaft-power ratio used for the performance constraints (Fig. 14a) directly affects the curves of the power-loading diagram (Fig. 8), where a higher value of φ (i.e., a higher share of OTWDP thrust) moves the constraint upward in the diagrams of the electric machines but downward in the gas-turbine diagram. The optimal shaft-power ratio during takeoff is comparable to the baseline value, remaining at around 0.2 to prevent the takeoff constraint from becoming the active sizing condition for the electrical machines. The shaft-power ratios in the OEI second-segment climb, OEI ceiling, and balked-landing constraints are lower than in the baseline configuration. This occurs because, in the baseline configuration, the electrical machines are sized by these performance constraints (see Fig. 8). However, these requirements can be alleviated by requesting more power from the primary propellers without affecting the gas-turbine size, which is limited by the takeoff constraint. The shaft-power ratio is also reduced in the landing constraint, which leads to a lower

maximum wing loading. This does not adversely affect the aircraft performance because the optimum wing loading is below the maximum wing loading. In other words, the shaft-power ratio and thrust-vectoring angle during landing do not affect the overall aircraft performance. In practice, this would imply that a smaller high-lift system could be used without a reduction in aircraft performance; i.e., $C_{L\max,\text{airframe}}$ can be reduced until the optimum design wing loading equals the maximum allowable wing loading.

Finally, Fig. 14b shows the improved power-control strategy throughout the nominal mission, once the size of the powertrain components has already been fixed by the constraint analysis. Here, the shaft-power ratio is adapted to maximize the overall efficiency, and therewith reduce fuel burn. Consequently, during the climb and cruise phases, the shaft-power ratio can be increased slightly to enhance the aeropropulsive benefits without exceeding the installed power of the electrical components. Finally, during descent, the shaft-power ratio tends toward the upper bound, although it has a negligible impact on the overall energy consumption because the thrust setting, and therefore fuel consumption, is minimal during descent.

C. Overall Performance Comparison

To provide a concluding discussion regarding the potential of OTWDP systems for regional transport aircraft, Table 4 compares

Table 4 Results of the OTWDP design-of-experiments study[a]

	Conventional		Baseline OTWDP		Optimal OTWDP	
M_{cr}	0.41	0.60	0.41	0.60	0.41	0.60
R, n miles	825	1500	825	1500	825	1500
x_P/c	— —	— —	0.80	0.80	0.776	0.782
N_2	— —	— —	24	24	36	32
D_P/c	— —	— —	0.25	0.25	0.17	0.19
i_P, deg	— —	— —	0	0	-5	-5
$\delta_{P,TO}$, deg	— —	— —	15	15	0.2	27.9
$\delta_{P,L}$, deg	— —	— —	45	45	21.2	44.2
$\delta_{P,bL}$, deg	— —	— —	45	45	20.8	21.7
W_{TO}/S_w, kN/m^2	4.00	4.00	4.50(+12%)	4.50(+12%))	4.04 (+0.9%)	3.91 (−2.4%)
$T_{c,\text{mean}} \times 10$	1.13	1.09	1.06 (−5.9%)	1.05 (−4.0%)	1.17 (+3.4%)	1.12 (+2.8%)
L/D	18.3	18.4	19.0 (+4.0%)	18.9 (+2.9%)	19.4 (+5.8%)	19.0 (+3.4%)
η_p	0.86	0.86	0.86 (−0.2%)	0.86 (−0.2%)	0.91 (+6.0%)	0.90 (+5.0%)
η_{PT}	0.33	0.33	0.32 (−3.4%)	0.32 (−3.1%)	0.31 (−4.3%)	0.32 (−3.4%)
ζ	5.12	5.14	5.13 (+0.2%)	5.11 (−0.5%)	5.50 (+7.3%)	5.39 (+4.8%)
m_{TO}, t	21.9	25.6	23.5 (+7.0%)	26.8 (+4.8%)	22.4 (+2.1%)	25.5 (-0.5%)
PREE	1.76	1.56	1.65 (−6.1%)	1.49 (−4.6%)	1.84 (+4.6%)	1.64 (+4.8%)

[a]Percentages expressed relative to the conventional aircraft for the same mission.

the design parameters and aircraft-level performance metrics of the baseline and optimized OTWDP configurations to the reference aircraft. Additional characteristics can be found in Table A1 in the Appendix. The optimal axial position and number of OTW propellers do not lie on the variables' bounds ($0.75 < x_P/c < 1.00$ and $20 < N_2 < 40$), indicating that the correct part of the design space has been explored in the DOE. This also suggests that larger OTW propellers are not necessarily better from an aeropropulsive perspective, contrary to what was initially hypothesized. Although larger propellers would have a higher isolated-propeller efficiency for the same total thrust requirement, the higher thrust coefficients required from smaller propellers enhance the $\Delta\eta_p$, ΔC_L, and ΔC_D terms, which appear to outweigh the benefits associated to a lower disk loading. This is reflected in the average thrust coefficient of all propellers throughout the mission $T_{c,mean}$; whereas in the baseline OTWDP configuration, it is 4–6% lower than the conventional aircraft due to the reduced drag, in the optimized configuration, it is increased by roughly 3% because the OTW propellers are purposely operated at a higher thrust setting during cruise. Moreover, the results show that, for the given approach-speed requirement and assumed $C_{L\,max,airframe}$, the thrust vectoring during the (balked) landing is not necessary. This is a consequence of the higher HEP-component power loadings that can be achieved at lower wing loadings, as was discussed earlier.

Table 4 shows that the average lift-to-drag ratio and propulsive efficiency of the optimized OTWDP aircraft are approximately 6% higher than the reference aircraft for the short-range mission. The benefits are reduced to 3.4 and 5%, respectively, for the long-range mission. Part of these benefits is forfeited in the transmission losses of the electric drivetrain, leading to overall increases of 7.3 and 4.8% in ζ for the short- and long-range missions, respectively. For the short-range mission, a portion of this benefit is required to compensate for the increase in aircraft weight due to the hybrid-electric powertrain. In total, this leads to a roughly 2% increase in takeoff mass, whereas the PREE is improved by 4.6%. For the long-range mission, the increase in powertrain weight is compensated for by the reduction in fuel weight; therefore, the takeoff mass is similar to the reference aircraft. In this case, a PREE increase of approximately 5% is achieved. The range of shaft-power ratios ($0.2 < \varphi < 0.5$) changes in aeropropulsive efficiency (9–12%), and changes in the PREE (~5%) obtained in this study are also in line with the values expected from Ref. [20].

D. Discussion: Potential Applications for OTWDP

These results indicate that hybrid-electric configurations with OTWDP can reduce the energy consumption of regional transport aircraft for the 2035 timeframe. However, a 5% reduction in energy consumption is most likely insufficient to justify a radical change in the overall layout of the aircraft. Furthermore, the sensitivity analysis of Sec. IV.B suggests a PREE uncertainty of approximately $\pm$ 5% due to uncertainty in the aerodynamic modeling of the OTWDP system alone. Hence, additional detailed studies on a particular OTWDP-system design would be required to determine whether the PREE benefit lies closer to 0% or to 10%. Moreover, the configuration analyzed in this study (Fig. 5) presents a relatively large center-of-gravity excursion, which is not modeled in the present class-I approach and may be a disadvantage as compared to conventional wing-mounted propeller configurations. Thus, a more detailed class-II design loop is required to assess the performance benefit more accurately. Nevertheless, the findings show that the aerodynamic benefits at the subsystem level can indeed lead to a benefit at the aircraft level. Based on these considerations, the following scenarios are identified as potential configurations where OTWDP may play a role in the future:

1. High-Efficiency Regional Transport

A regional aircraft with OTWDP could present a more significant reduction in energy consumption if the aeropropulsive benefits are increased beyond the ones estimated in this study.

This may be achieved with a more optimal design of the OTWDP geometry, or if the full span of the wing can be covered without significant penalties in the structural weight or stability and control of the aircraft. Advancements in HEP-component technology also play an important role in this sense, because the PREE benefits increase significantly with the efficiency and specific power of the electrical components [20]. Moreover, as the aviation industry gains experience with the operation and certification of (hybrid-) electric powertrain components for smaller aircraft, the entry barriers for such technologies for larger regional aircraft will be reduced.

2. Low-Noise Regional Transport

This is considered separately from the previous point because the optimum OTWDP design in terms of aerodynamic efficiency (propellers near the trailing edge) is likely to differ considerably from the optimum design in terms of community noise. However, if the propellers are ducted and placed more forward to exploit the shielding capabilities of the wing, a low-noise configuration may be achieved. In that case, the primary propellers would also have to be installed in a low-noise configuration: for example, above a U tail [59] or as ducted propellers [60,61]. Another advantage of OTWDP with respect to a conventional twin turboprop in this regard is the possibility to increase the total disk area, which may allow lower blade-tip Mach numbers for a given thrust requirement.

3. Small Fully Electric Aircraft

If smaller, fully electric aircraft are used in the future for inter- or intracity transport due to lower operating costs or the absence of in-flight emissions, then considerations such as short takeoff and landing capabilities or flyover noise will play a relatively larger role [62]. In that case, OTWDP can present several advantages over conventional or LEDP configurations, without significantly increasing the weight of the already electric powertrain. In addition to a potential increase in cruise performance, OTWDP can increase the high-lift capabilities by deflecting the propeller and flap and, in a limit case, enable vertical takeoff and landing operations. Furthermore, the noise shielding can be an important advantage over leading-edge configurations when operating close to urban areas. Depending on the type of runway, the improved shielding from foreign-object damage may also constitute an additional benefit. Also for these applications, it is important to keep in mind that the optimal OTWDP designs in terms of cruise performance, high-lift performance, and noise production are likely to differ considerably; therefore, not all benefits can be maximized simultaneously.

4. Long-Haul Transport

The results of this study and the previous ones [20] confirm that the increased aeropropulsive benefit leads to a larger benefit at the aircraft level for longer ranges. However, long-haul missions typically require transonic cruise speeds. In these conditions, OTWDP would require divergent ducts and present significant challenges due to shock formation on the upper side of the wing [63]. However, for very low diameter-to-chord ratios, it may still provide benefits. This may be possible, for example, in a blended-wing/body configuration [64]. However, in that case, the diameter of the propulsors is comparable to the height of the boundary layer, and many of the aerodynamic observations made in the present study no longer hold or are no longer dominant. Instead, more attention has to be paid to the boundary-layer ingestion effects.

VI.   Conclusions

The study presented in this paper analyzes how the aerodynamic benefits of over-the-wing distributed propulsion at the subsystem level translate into an aeropropulsive benefit at the aircraft level, and how that in turn affects the energy consumption

of the aircraft. For the case study, a partial-turboelectric regional transport aircraft featuring aft-mounted propellers and an OTWDP system is compared to a conventional twin-turboprop configuration. Both aircraft are sized from a class-I perspective for an entry into service of circa 2035. To account for the aeropropulsive coupling of the OTWDP system, a simplified numerical method is developed. The method is intended for cruise conditions, and it models the aerodynamic interaction between propellers and the wing, neglecting other elements such as pylons, nacelles, or any potential ducts. A validation study with experimental data is performed to identify the applicability and limitations of the model. The comparisons show that the numerical model captures the changes in lift, drag, and propulsive efficiency with sufficient accuracy for preliminary-sizing purposes. However, the model does not provide realistic results if flow separation occurs beneath the propeller.

For the model geometry employed in the experimental campaign, a 23% and 51% increase in the wing lift-to-drag ratio are found for low and moderate thrust settings, respectively. For the same geometry in typical cruise conditions, the numerical model predicts a 45% increase in the sectional wing lift-to-drag ratio, which is accompanied by a 12% reduction in (propeller) propulsive efficiency. These effects are incorporated in the aircraft sizing process, and a design of experiments is carried out to determine a well-performing power-control strategy (i.e., shaft-power ratio) and OTWDP geometry (e.g., diameter-to-chord ratio, axial propeller position, and incidence angle). The resultant best-performing configuration presents a shaft-power ratio of approximately $\varphi = 0.2$ in the sizing condition, as well as an OTWDP system with 32–36 propulsors located at $x_P/c = 0.78$ with a diameter-to-chord ratio of 0.17–0.19, depending on the mission. In that case, the average aeropropulsive efficiency of the aircraft is found to increase by 12 and 9% relative to the reference aircraft for short- ($M_{cr} = 0.41$ and $R = 825$ n miles) and medium-range ($M_{cr} = 0.60$ and $R = 1500$ n miles) missions, respectively. The takeoff mass of the OTWDP configuration is 2% higher than the reference for the short-range mission; whereas for the medium-range mission, the reduction in fuel weight compensates for the increase in powertrain weight and leads to a takeoff mass similar to the reference aircraft. In both cases, the energy efficiency of the OTWDP configuration is approximately 5% higher than the reference aircraft, although a $\pm 5\%$ uncertainty exists due to uncertainty in the aerodynamic modeling alone.

The 5% reduction in energy consumption is most likely insufficient to justify the additional complexity of the OTWDP system and the powertrain required to drive it. Nevertheless, the results confirm that the aerodynamic benefits of OTWDP at component level can indeed lead to a nonnegligible aeropropulsive benefit at the aircraft level. To exploit these benefits (not only for regional aircraft but also for potential applications on smaller, fully electric aircraft or long-haul aircraft), additional detailed studies are required. Such studies should perform a more detailed design and shape optimization of the OTWDP system to reduce the uncertainty regarding the aerodynamic performance of the system, as well as to estimate the acoustic characteristics of a realistic geometry. Investigations into other disciplines, such as the effect on control and stability or wing structural weight, are also required. In all these cases, the duct may play an important role. However, if these studies can confirm aerodynamic benefits equal to or greater than the ones encountered here and additionally demonstrate the noise-shielding capabilities, then there is a strong case for OTWDP applications on future energy-efficient aircraft configurations.

Appendix: Aircraft Sizing Data

Table A1 Powertrain and wing characteristics obtained[a,b]

	Conventional aircraft		Baseline OTWDP		Optimal OTWDP	
M_{cr}	0.41	0.60	0.41	0.60	0.41	0.60
R, n miles	825	1500	825	1500	825	1500
h_{cr}, ft	22,400	39,800	19,100	36,900	22,100	40,000
No. of primary propulsors	2	2	2	2	2	2
No. of secondary propulsors	N/A	N/A	24	24	36	32
Takeoff mass, t	21.9	25.6	23.5	26.8	22.4	25.5
Payload mass, t	7.5	7.5	7.5	7.5	7.5	7.5
Operative empty mass, t	12.3	14.2	13.7	15.2	12.8	14.3
Wing mass, t	2.2	2.6	2.3	2.6	2.3	2.6
Gas turbine mass, t	1.2	2.3	1.5	2.2	1.2	2.2
Generator mass, kg	N/A	N/A	98	112	72	96
Rectifier mass, kg	N/A	N/A	93	106	51	68
Electromotor mass, kg	N/A	N/A	136	155	75	100
Inverter mass, kg	N/A	N/A	67	77	49	65
Additional PMAD mass, kg	N/A	N/A	118	135	74	98
Fuel mass, t	2.1	3.9	2.3	4.1	2.1	3.7
Wing loading, kN/m^2	4.0	4.0	4.5	4.5	4.0	3.9
Wing area, m^2	53.8	62.7	51.2	28.5	54.4	64.0
Wingspan, m	25.4	27.4	24.8	26.5	25.5	27.7
Diameter primary propellers, m	3.7	4.0	3.1	3.3	3.2	3.5
Diameter secondary propellers, m	N/A	N/A	0.52	0.56	0.36	0.44
Gas turbine W_{TO}/P, N/kW	47.9	27.8	40.4	30.9	48.2	29.1
Generator W_{TO}/P, N/kW	N/A	N/A	130	130	226	193
Electromotor W_{TO}/P, N/kW	N/A	N/A	180	180	235	201
Gas turbine power, MW	4.5	9.0	5.7	8.5	4.6	8.6
Generator power, MW	N/A	N/A	1.8	2.0	1.0	1.3
Electromotor power, MW	N/A	N/A	1.3	1.5	0.9	1.2

[a]Powertrain properties refer to the total installed power or mass, not per component instance.
[b]N/A denotes "not applicable."

Table A2 Overview of the OTWDP design parameters varied in the DOE[a]

		Bounds		Baseline OTWDP		Optimal OTWDP	
		Lower	Upper				
Mission requirements	M_{cr}	——	——	0.41	0.60	0.41	0.60
	R, n mile	——	——	825	1500	825	1500
Geometry	x_P/c	0.75	1.00	0.80	0.80	0.776	0.782
	b_{dp}/b[b]	0.25	0.75	0.53	0.53	0.53	0.53
	N_2	20	40	24	24	36	32
	i_P, deg	-5	10	0	0	−5	−5b
	$\delta_{P,TO}$, deg	0	45	15	15	0.2	27.9
	$\delta_{P,L}$, deg	0	45	45	45	21.2	44.2
	$\delta_{P,bL}$, deg	45	45	45	45	20.8	21.7
Design point	$(W_{TO}/S_w)/(W_{TO}/S_w)_{max}$	0.4	1	1.00	1.00	0.99	0.88
Performance constraints	φ_{cr}	0	1	0.50	0.50	0.44	0.44
	φ_{TO}	0	1	0.20	0.20	0.21	0.25
	φ_L	0	1	1.00	1.00	0.26	0.99
	φ_{ssc}	0	1	0.50	0.50	0.28	0.38
	φ_{cI}	0	1	0.50	0.50	0.29	0.40
	φ_{bL}	0	1	0.50	0.50	0.38	0.47
	$\xi_{GT,cr}$	——	——	0.90	0.90	0.90	0.90
	$\xi_{GT,TO}$	——	——	1.00	1.00	1.00	1.00
	$\xi_{GT,L}$	——	——	0.90	0.90	0.90	0.90
	$\xi_{GT,ssc}$	——	——	1.00	1.00	1.00	1.00
	$\xi_{GT,cI}$	——	——	1.00	1.00	1.00	1.00
	$\xi_{GT,bL}$	——	——	1.00	1.00	1.00	1.00
Climb	φ_1	0	1	0.50	0.50	0.26	0.18
	φ_2	0	1	0.50	0.50	0.29	0.21
	$\xi_{GT,1}$	——	——	0.80	0.80	0.80	0.80
	$\xi_{GT,2}$	——	——	0.90	0.90	0.90	0.90
Cruise	φ_1	0	1	0.50	0.50	0.58	0.50
	φ_2	0	1	0.50	0.50	0.61	0.53
Descent	φ_1	0	1	0.50	0.50	0.99	0.99c
	φ_2	0	1	0.50	0.50	0.99	0.99c
	$\xi_{GT,1}$	——	——	0.05	0.05	0.05	0.05
	$\xi_{GT,2}$	——	——	0.05	0.05	0.05	0.05
Loiter	φ_1	0	1	0.50	0.50	0.38	0.43
	φ_2	0	1	0.50	0.50	0.42	0.45

[a]The gas-turbine throttle setting is included for reference, although it was not varied. Subscripts "1" and "2" indicate the start and end of the mission segment, respectively. Climb, cruise, and descent (φ and ξ_{GT}) settings are applied to both the nominal mission and the diversion.
[b]This parameter was varied in the geometry-oriented DOE but kept constant in the final DOE.
[c]These parameters were kept constant in the final DOE of the long-range mission because previous results showed that they would tend toward the bounds.

Acknowledgments

References

[1] Lee, D. S., Fahey, D., Skowron, A., Allen, M. R., Burkhardt, U., Chen, Q., Doherty, S. J., Freeman, S., Forster, P. M., Fuglestvedt, J., and Gettelman, A., "The Contribution of Global Aviation to Anthropogenic Climate Forcing for 2000 to 2018," *Atmospheric Environment*, Vol. 244, Jan. 2021, Paper 117834.
https://doi.org/10.1016/j.atmosenv.2020.117834

[2] Anon., "Realising Europe's Vision for Aviation: Strategic Research and Innovation Agenda," Vol. 1, Advisory Council for Aviation Research and Innovation in Europe, 2012.

[3] Bonet, J. T., Schellenger, H. G., Rawdon, B. K., Elmer, K. R., Wakayama, S. R., Brown, D. L., and Guo, Y., "Environmentally Responsible Aviation (ERA) Project-$N+2$ Advanced Vehicle Concepts Study and Conceptual Design of Subscale Test Vehicle (STV): Final Report," NASA CR-2011-216519, Dec. 2011.

[4] Green, J. E., "Air Travel-Greener by Design. Mitigating the Environmental Impact of Aviation: Opportunities and Priorities," *Aeronautical Journal*, Vol. 109, No. 1099, 2005, pp. 361–418.
https://doi.org/10.1017/S0001924000000841

[5] *Engineering, and Medicine, Commercial Aircraft Propulsion and Energy Systems Research: Reducing Global Carbon Emissions*, National Academies Press, Washington, D.C., 2016, Chap. 2.
https://doi.org/10.17226/23490

[6] Clean Aviation Joint Undertaking, "Strategic Research and Innovation Agenda," Dec. 2021, https://www.clean-aviation.eu/strategic-research-and-innovation-agenda-sria [retrieved 3 Feb. 2023].

[7] Epstein, A. H., and O'Flarity, S. M., "Considerations for Reducing Aviation's with Aircraft Electric Propulsion," *Journal of Propulsion*

and Power, Vol. 35, No. 3, 2019, pp. 572–582.
https://doi.org/10.2514/1.B37015

[8] Gnadt, A. R., Speth, R. L., Sabnis, J. S., and Barrett, S. R. H., "Technical and Environmental Assessment of All-Electric 180-Passenger Commercial Aircraft," *Progress in Aerospace Sciences*, Vol. 105, Feb. 2019, pp. 1–30.
https://doi.org/10.1016/j.paerosci.2018.11.002

[9] Schafer, A. W., Barrett, S. R. H., Doyme, K., Dray, L. M., Gnadt, A. R., Self, R., O'Sullivan, A., Synodinos, A. P., and Torija, A. J., "Technological, Economic and Environmental Prospects of All-Electric Aircraft," *Nature Energy*, Vol. 4, No. 2, 2019, pp. 160–166.
https://doi.org/10.1038/s41560-018-0294-x

[10] Hoogreef, M. F. M., de Vries, R., Sinnige, T., and Vos, R., "Synthesis of Aero-Propulsive Interaction Studies Applied to Conceptual Hybrid-Electric Aircraft Design," *2020 AIAA Aerospace Sciences Meeting*, AIAA Paper 2020-0503, Jan. 2020.
https://doi.org/10.2514/6.2020-0503

[11] Kim, H. D., "Distributed Propulsion Vehicles," *27th Congress of the International Council of the Aeronautical Sciences*, ICAS Paper 2010-1.1.3, Sept. 2010.

[12] Borer, N. K., Patterson, M. D., Viken, J. K., Moore, M. D., Bevirt, J., Stoll, A. M., and Gibson, A. R., "Design and Performance of the NASA SCEPTOR Distributed Electric Propulsion Flight Demonstrator," *16th AIAA Aviation Technology, Integration, and Operations Conference*, AIAA Paper 2016-3920, June 2016.
https://doi.org/10.2514/6.2016-3920

[13] Biser, S., Filipenko, M., Boll, M., Kastner, N., Atanasov, G., Hepperle, M., Keller, D., Vechtel, D., and Noe, M., "Design Space Exploration Study and Optimization of a Distributed Turbo-Electric Propulsion System for a Regional Passenger Aircraft," *AIAA Propulsion and Energy Forum*, AIAA Paper 2020-3592, Aug. 2020.
https://doi.org/10.2514/6.2020-3592

[14] Johnson, J. L., Jr., and White, E. R., "Exploratory Low-Speed Wind-Tunnel Investigation of Advanced Commuter Configurations Including an Over-the-Wing Propeller," *AIAA Aircraft Design, Systems and Technology Meeting*, AIAA Paper 1983-2531, Oct. 1983.
https://doi.org/10.2514/6.1983-2531

[15] Müller, L., Kožulović, D., Hepperle, M., and Radespiel, R., "The Influence of the Propeller Position on the Aerodynamics of a Channel Wing," *Deutscher Luft-und Raumfahrt Kongress*, Berlin, Germany, Sept. 2012.

[16] Beck, S. C., Müller, L., and Langer, S. C., "Numerical Assessment of the Vibration Control Effects of Porous Liners on an Over-the-Wing Propeller Configuration," *CEAS Aeronautical Journal*, Vol. 7, No. 2, 2016, pp. 275–286.
https://doi.org/10.1007/s13272-016-0186-3

[17] de Vries, R., van Arnhem, N., Avallone, F., Ragni, D., Vos, R., Eitelberg, G., and Veldhuis, L. L. M., "Experimental Investigation of Over-the-Wing Propeller–Boundary-Layer Interaction," *AIAA Journal*, Vol. 59, No. 6, 2021, pp. 2169–2182.
https://doi.org/10.2514/1.J059770

[18] Bölk, S. A., de Vries, R., van Arnhem, N., and Veldhuis, L. L. M., "Numerical Investigation of Propeller–Flap Interaction in Inclined Over-the-Wing Distributed-Propulsion Systems," *AIAA SciTech 2021 Forum*, AIAA Paper 2021-0603, Jan. 2021.
https://doi.org/10.2514/6.2021-0603

[19] Veldhuis, L. L. M., "Propeller Wing Aerodynamic Interference," Ph.D. Dissertation, Delft Univ. of Technology, Delft, The Netherlands, 2005.

[20] de Vries, R., Hoogreef, M. F. M., and Vos, R., "Aeropropulsive Efficiency Requirements for Turboelectric Transport Aircraft," *AIAA SciTech 2020 Forum*, AIAA Paper 2020-0502, Jan. 2020.
https://doi.org/10.2514/6.2020-0502

[21] de Vries, R., Brown, M., and Vos, R., "Preliminary Sizing Method for Hybrid-Electric Distributed-Propulsion Aircraft," *Journal of Aircraft*, Vol. 56, No. 6, 2019, pp. 2172–2188.
https://doi.org/10.2514/1.C035388

[22] Torenbeek, E., *Synthesis of Subsonic Airplane Design*, Delft Univ. Press, Delft, The Netherlands, 1982.

[23] Raymer, D. P., *Aircraft Design: A Conceptual Approach*, AIAA Education Series, AIAA, Reston, VA, 2002.
https://doi.org/10.2514/4.869112

[24] Roskam, J., "Airplane Design, Part I: Preliminary Sizing of Airplanes," DARcorp., Lawrence, KS, 1985.

[25] Finger, D. F., de Vries, R., Vos, R., Braun, C., and Bil, C., "Cross-Validation of Hybrid-Electric Aircraft Sizing Methods," *Journal of Aircraft*, Vol. 59, No. 3, Jan. 2022, pp. 1–19.
https://doi.org/10.2514/1.C035907

[26] Habermann, A. L., "Effects of Distributed Propulsion on Wing Mass in Aircraft Conceptual Design," *AIAA Aviation 2020 Forum*, AIAA Paper 2020-2625, June 2020.

[27] Nguyen Van, E., Alazard, D., Döll, C., and Pastor, P., "Co-Design of Aircraft Vertical Tail and Control Laws with Distributed Electric Propulsion and Flight Envelop Constraints," *CEAS Aeronautical Journal*, Vol. 12, No. 1, 2021, pp. 101–113.
https://doi.org/10.1007/s13272-020-00481-8

[28] de Vries, R., "Hybrid-Electric Aircraft with Over-the-Wing Distributed Propulsion: Aerodynamic Performance and Conceptual Design," Ph.D. Dissertation, Delft Univ. of Technology, Delft, The Netherlands, 2022.

[29] Boermans, L. M. M., and Rutten, P. B., "Two-Dimensional Aerodynamic Characteristics of Airfoil NLF-MOD22 with Fowler Flap," Delft Univ. of Technology Internal Rept. LSW-95-3, Delft, The Netherlands, 1995.

[30] Marcus, E. A. P., de Vries, R., Raju Kulkarni, A., and Veldhuis, L. L. M., "Aerodynamic Investigation of an Over-the-Wing Propeller for Distributed Propulsion," *2018 AIAA Aerospace Sciences Meeting*, AIAA Paper 2018-2053, Jan. 2018.
https://doi.org/10.2514/6.2018-2053

[31] de Vries, R., van Arnhem, N., Sinnige, T., Vos, R., and Veldhuis, L. L. M., "Aerodynamic Interaction Between Propellers of a Distributed-Propulsion System in Forward Flight," *Aerospace Science and Technology*, Vol. 118, Nov. 2021, Paper 107009.
https://doi.org/10.1016/j.ast.2021.107009

[32] van Arnhem, N., de Vries, R., Sinnige, T., Vos, R., Eitelberg, G., and Veldhuis, L. L. M., "Engineering Method to Estimate the Blade Loading of Propellers in Nonuniform Flow," *AIAA Journal*, Vol. 58, No. 12, 2020, pp. 5332–5346.
https://doi.org/10.2514/1.J059485

[33] Yoon, S. S., and Heister, S. D., "Analytical Formulas for the Velocity Field Induced by an Infinitely Thin Vortex Ring," *International Journal for Numerical Methods in Fluids*, Vol. 44, No. 6, 2004, pp. 665–672.
https://doi.org/10.1002/fld.666

[34] Katz, J., and Plotkin, A., *Low-Speed Aerodynamics*, 13th ed., Cambridge Univ. Press, Cambridge, England, U.K.,2001, Chap. 11.
https://doi.org/10.1017/CBO9780511810329

[35] Drela, M., "XFOIL: An Analysis and Design System for Low Reynolds Number Airfoils," *Low Reynolds Number Aerodynamics. Lecture Notes in Engineering*, Vol. 54, edited by T. J. Mueller, Springer, Berlin, Germany, 1989.
https://doi.org/10.1007/978-3-642-84010-4_1

[36] Isikiveren, A. T., "Guidelines for Analysis of Hybrid Electric Aircraft System Studies: Nomenclature, Pictographic Representations, Standalone and Combined Properties and Attributes, Metrics, and Figures of Merit," *AIAA Aircraft Electrified Propulsion and Power (AEPP) Working Group* Action Item 40, Reston, VA, 2019.

[37] Torenbeek, E., *Optimum Cruise Performance of Subsonic Transport Aircraft*, Delft Univ. Press, Delft, The Netherlands, 1998, Chap. 4.

[38] de Vries, R., Hoogreef, M. F. M., and Vos, R., "Preliminary Sizing of a Hybrid-Electric Passenger Aircraft Featuring Over-the-Wing Distributed-Propulsion," *2019 AIAA Aerospace Sciences Meeting*, AIAA Paper 2019-1811, Jan. 2019.
https://doi.org/10.2514/6.2019-1811

[39] Lambert, M., and Jane, F. T., *Jane's All the World's Aircraft:1990–91*, 81st ed., Jane's Information Group, Sept. 1990.

[40] Nicolosi, F., Corcione, S., Trifari, V., Cusati, V., Ruocco, M., and Della Vecchia, P., "Performance Evaluation and DOC Estimation of an Innovative Turboprop Configuration," *2018 Aviation Technology, Integration, and Operations Conference*, AIAA Paper 2018-3662, June 2018.
https://doi.org/10.2514/6.2018-3662

[41] van Arnhem, N., de Vries, R., Sinnige, T., Vos, R., and Veldhuis, L. L. M., "Aerodynamic Performance and Static Stability Characteristics of Aircraft with Tail-Mounted Propellers," *Journal of Aircraft*, Vol. 59, No. 2, 2022, pp. 415–432.
https://doi.org/10.2514/1.C036338

[42] Kenway, G. K. W., Henderson, R., Hicken, J. E., Kuntawala, N. B., Zingg, D. W., Martins, J. R. R. A., and McKeand, R. G., "Reducing Aviation's Environmental Impact Through Large Aircraft For Short Ranges," *48th AIAA Aerospace Sciences Meeting*, AIAA Paper 2010-1015, Jan. 2010.
https://doi.org/10.2514/6.2010-1015

[43] Randt, N. P., "Perspectives of Turboprop Aircraft: A Stakeholder-Oriented Evaluation Using Scenario Planning," *63rd German Aerospace Congress*, Augsburg, Germany, Sept. 2014.

[44] "Certification Specifications and Acceptable Means of Compliance for Large Aeroplanes CS25," Amendment 21, European Aviation Safety Agency, Cologne, Germany, 2018.

[45] Torenbeek, E., *Advanced Aircraft Design: Conceptual Design, Analysis and Optimization of Subsonic Civil Airplanes*, Wiley, Hoboken, NJ, 2013, Chap. 9.

[46] Reuland, R. S., "Pusher Turboprop Installation Technology for the Embraer CBA-123 Vector," *SAE Transactions*, Vol. 100, Sec. 1: *Journal of Aerospace*, Pt. I, 1991, pp. 222–228.

[47] Goldsmith, I. M., "A Study to Define the Research and Technology Requirements for Advanced Turbo/Propfan Transport Aircraft," NASA CR 166138, Feb. 1981.

[48] Sinnige, T., Ragni, D., Eitelberg, G., and Veldhuis, L. L. M., "Mitigation of Pusher-Propeller Installation Effects by Pylon Trailing-Edge Blowing," *Journal of Aircraft*, Vol. 54, No. 1, 2017, pp. 292–300.
https://doi.org/10.2514/1.C034000

[49] Vos, R., and Hoogreef, M. F. M., "System-Level Assessment of Tail-Mounted Propellers for Regional Aircraft," *31st International Congress of the Aeronautical Sciences*, ICAS Paper 2018-0065, Sept. 2018.

[50] Cooper, R. K., McCann, W. J., and Chapleo, A. Q., "Over Wing Propeller Aerodynamics," *18th Congress of the International Council of the Aeronautical Sciences*, Vol. 18, ICAS Paper 92-3.2.2, Sept. 1992, pp. 266–273.

[51] Nathen, P., "Architectural Performance Assessment of an Electric Vertical Take-Off and Landing (e-VTOL) Aircraft Based on a Ducted Vectored Thrust Concept," April 2021.

[52] Perry, A. T., Ansell, P. J., and Kerho, M. F., "Aero-Propulsive and Propulsor Cross-Coupling Effects on a Distributed Propulsion System," *Journal of Aircraft*, Vol. 55, No. 6, 2018, pp. 2414–2426.
https://doi.org/10.2514/1.C034861

[53] Hermetz, J., Ridel, M., and Döll, C., "Distributed Electric Propulsion for Small Business Aircraft: A Concept-Plane for Key-Technologies Investigations," *30th ICAS Congress*, ICAS Paper 2016-0461, 2016.

[54] Bento, H. F. M., de Vries, R., and Veldhuis, L. L. M., "Aerodynamic Performance and Interaction Effects of Circular and Square Ducted Propellers," *AIAA SciTech 2020 Forum*, AIAA Paper 2020-1029, Jan. 2020.
https://doi.org/10.2514/6.2020-1029

[55] Black, D., Wainauski, H., and Rohrbach, C., "Shrouded Propellers—A Comprehensive Performance Study," *AIAA 5th Annual Meeting and Technical Display*, 1968-0994, Oct. 1968.
https://doi.org/10.2514/6.1968-994

[56] Dekkers, N., "Aero-Propulsive Analysis of an Over-the-Wing Distributed Propulsion System," M.Sc. Thesis, Delft Univ. of Technology, Delft, The Netherlands, 2021.

[57] Broadbent, E. G., "Noise Shielding for Aircraft," *Progress in Aerospace Sciences*, Vol. 17, Jan. 1976, pp. 231–268.
https://doi.org/10.1016/0376-0421(76)90009-9

[58] Jansen, R. H., Bowman, C., Jankovsky, A., Dyson, R., and Felder, J., "Overview of NASA Electrified Aircraft Propulsion Research for Large Subsonic Transports," *53rd AIAA/SAE/ASEE Joint Propulsion Conference*, AIAA Paper 2017-4701, July 2017.
https://doi.org/10.2514/6.2017-4701

[59] Sanders, L., Mincu, D.-C., Vitagliano, P. L., Minervino, M., Kennedy, J., and Bennett, G., "Prediction of the Acoustic Shielding by Aircraft Empennage for Contrarotating Open Rotors," *International Journal of Aeroacoustics*, Vol. 16, Nos. 7–8, 2017, pp. 626–648.
https://doi.org/10.1177/1475472X17734334

[60] Hubbard, H. H., "Sound Measurements for Five Shrouded Propellers at Static Conditions," NACA TN-2024, 1950.

[61] Dittmar, J. H., "An Estimate of the Noise Shielding on the Fuselage Resulting from Installing a Short Duct Around an Advanced Propeller," NASA TM-100262, 1988.

[62] Antcliff, K., Borer, N., Sartorius, S., Saleh, P., Rose, R., Gariel, M., Oldham, J., Courtin, C., Bradley, M., Roy, S., and Lynch, B., "Regional Air Mobility: Leveraging Our National Investments to Energize the American Travel Experience," NASA, April 2021.

[63] Wick, A. T., Hooker, J. R., Hardin, C. J., and Zeune, C. H., "Integrated Aerodynamic Benefits of Distributed Propulsion," *53rd AIAA Aerospace Sciences Meeting*, AIAA Paper 2015-1500, Jan. 2015.
https://doi.org/10.2514/6.2015-1500

[64] Felder, J. L., Kim, H. D., and Brown, G. V., "Turboelectric Distributed Propulsion Engine Cycle Analysis for Hybrid-Wing-Body Aircraft," *47th AIAA Aerospace Sciences Meeting*, AIAA Paper 2009-1132, Jan. 2009.
https://doi.org/10.2514/6.2009-1132